INTERIM REPORT

Accession No. ___
ORNL/MRBT-5

Contract Program or Project Title: MULTIROD BURST TEST PROGRAM

Subject of this Document: Preliminary Results of B-5 (8 × 8) Bundle Test

Type of Document: Quick-look Report

Authors: R. H. Chapman, J. L. Crowley, R. F. Haynes and A. W. Longest

Date of Document: July 14, 1980

Responsible NRC Individual and NRC Office or Division: M. L. Picklesimer, Fuel Behavior Branch, Division of Reactor Safety Research, Office of Nuclear Regulatory Research

Prepared for the
U.S. Nuclear Regulatory Commission
Washington, D.C. 20555
Under Interagency Agreements DOE 40-551-75 and 40-552-75
NRC FIN No. B0120

Oak Ridge National Laboratory
Oak Ridge, Tennessee 37830
operated by
Union Carbide Corporation
for the
Department of Energy

INTERIM REPORT

Introduction

The 8 × 8 (B-5) bundle burst test was performed successfully about 6:00 p.m. on May 30, two days ahead of the scheduled milestone completion date. The heating rate and initial conditions were approximately the same as used in the B-3 (4 × 4) test in order to obtain information on the effect of test array size on deformation and rod-to-rod interactions.

Due to a severe leak that developed in the lower seal of a simulator prior to the test, one tube (No. 62) in the outer ring of simulators was unpressurized; however, it was heated to give the proper temperature conditions. All the 63 pressurized tubes burst, and the average burst temperature was about 770°C. The first tube burst after about 44.0 s of heating; the last tube burst about 5.6 s later. Power was applied to the bundle approximately 48.1 s.

Figure 1 shows a simplified drawing of the B-5 test assembly. As indicated in Section A-A of the figure, the shroud was constructed of thin (0.1 mm thick) Inconel, with a highly reflective plating, and was backed by insulating material and a strong structure to withstand radial forces during the test transient. The shroud was spaced one-half of a coolant-channel-distance away from the outer rod surfaces. This would permit some deformation of these simulators before contact, but would prevent outward movement of the simulators.

Figure 2 gives pertinent details of the fuel pin simulators. The fuel simulators (internal heaters) were selected from the lot produced in our Fuel Rod Simulator Technology Development Laboratory. The axial heat generation profile of these simulators, as determined by pretest infrared characterization scans, is more uniform than that in the simulators used in the 4 × 4 tests. The highest quality simulators were selected for interior positions in the array.

Each fuel pin simulator was instrumented with a fast response, strain-gage-type, pressure transducer and four Inconel sheathed (0.71-mm O.D.), type K thermocouples with ungrounded junctions. The thermocouples were spot-welded to the inside of the Zircaloy-4 tubes (10.9-mm O.D. × 0.635-mm wall thickness) at axial and azimuthal positions shown in Fig. 3.

The figure also gives thermocouple identifications for use in subsequent figures for which the nomenclature TE 10-4 identifies the No. 4 thermocouple in the No. 10 simulator. Figure 4 shows the axial distribution of the simulator thermocouples. As noted in Fig. 3, four 0.25-mm-diam bare wire, type S thermocouples were attached to the outside surface of each of four simulators (Nos. 5, 28, 39, and 44) in an attempt to obtain azimuthal temperature gradient information. These thermocouples were equally spaced around the tubes at the 48 cm elevation. An internal thermocouple was also located in each of these simulators at this elevation. Three of the external thermocouples on rod No. 39 became detached during subsequent assembly of the shroud panels. Although performance of the remaining external thermocouples was less than desirable, good information was obtained from the thermocouples on rod No. 28.

Sixteen, 0.076-mm-diam, bare wire, type S thermocouples were spot welded directly on the outside surface of the thin shroud surrounding the rod array. Four thermocouples were attached to each side at positions shown in Fig. 3 in an attempt to obtain information on both the axial and circumferential temperature distributions. The shroud thermocouple identifications are also given in the figure for use in subsequent temperature plots. The performance of these was not as good as expected; however, good information was obtained from all four thermocouples on the west face of the shroud.

Three thermocouples (TE-320 through TE-322) were located in the tube matrix at the 107-cm elevation (centerline elevation of the steam inlet nozzle) to obtain inlet steam temperature measurements across the bundle. Five thermocouples (TE-323 through TE-327) were dispersed in the tube matrix at the bottom of the heated zone (0-cm elevation) to obtain outlet steam temperature measurements at the center and at the center of the four quadrants of the bundle at this elevation. Figure 5 shows the identifications and locations. The thermocouples were 0.71-mm-diam, stainless steel sheathed, type K with insulated junctions.

Millivolt signals from the pressure transducers, thermocouples, and electrical power measuring instruments were recorded on magnetic tape by a

computer controlled data acquisition system (CCDAS) for subsequent analysis. This report summarizes some of the quick-look data obtained immediately after the test and presents a selection of photographs of the bundle.

Test Operations

Heatup of the test assembly was initiated early in the afternoon of May 29; the temperature was near 200°C at the end of the work shift. Power adjustments to the vessel heaters were made to maintain the temperature near this value during the next 12 hours to avoid temperature cycling the test assembly. About 4:00 a.m. on May 30, power to the vessel heaters was increased and superheated steam was admitted to the vessel in the approach to the initial test temperature. Throughout this phase of operation periodic leak checks indicated the simulator seals were performing very well, (i.e., less than 10 kPa pressure loss per min at 7600 kPa and ~330°C).

After thermal equilibration (about 335°C) of the test assembly was attained, the simulators were pressurized to approximately 7700 kPa, and a short powered run (~9.0 s transient) was conducted at 10:45 a.m. to ascertain that the data acquisition system and all the instrumentation were functioning properly and that the performance of the test components was as expected. Examination and evaluation of the quick-look data from this short transient (the temperature of the simulators increased to about 390°C) indicated slight adjustments were needed to achieve the desired heating rate. In particular, the applied voltage setting was adjusted upward in an attempt to achieve the desired heating rate of 10 K/s.

During the high temperature hold time (approximately 6 s) between the pretest power-bump and the burst test, the lower seal on simulator 62 developed a gross leak, which was determined after the test to be at the copper gasket which gave so much trouble in the pretest checkout operation of the B-3 test. The magnitude of the leak was such that its effect could not be counteracted by inflow of helium. Since this simulator is located in the outer ring of the bundle (see Fig. 3), the influence of its deformation on the remainder of the simulators should be small, and it was

decided to continue the test with the simulator unpressurized. However, it was heated so that the proper temperature boundary conditions would be preserved. All the other simulators were tested in the usual manner, i.e., with the isolation valves to the supply header closed to provide a constant gas mass inventory in each pressurized simulator during the transient.

During the powered portion of the transient, superheated steam flowed downward through the test assembly at the same mass flux as used in the B-3 test — about 288 $g/s \cdot m^2$. Inlet steam conditions of ~355°C and 290 kPa (absolute) resulted in a Reynolds Number of 140. These inlet conditions remained essentially constant until disrupted by escaping helium from the bursting tubes and from the opening of the posttest steam cooling valves. When power to the bundle was terminated, the steam flow was increased to an estimated minimum of 15 g/s to effect rapid cooldown of the bundle.

Following stabilization of the bundle temperature at ~335°C, all the fuel pin simulators except No. 62 were pressurized simultaneously to ~11600 kPa and isolated from the supply header. The header was vented and the leak rate of each of the 15 simulators was checked over a 2-min period, with the pressure loss being about 10 kPa/min. With these initial conditions established, the test transient was initiated.

Termination of the powered portion of the test could be initiated by any of four actions: (a) CCDAS action resulting from a signal that 60 of the 64 simulators had burst, (b) CCDAS action that 150 simulator thermocouples had exceeded the upper temperature limit (50°C above the anticipated burst temperature) on each of three successive data scans, (c) a timer that limited the transient to 60 s, and (d) operator override. It was decided to program criterion (a) to terminate power to the bundle after 60 bursts (with the expectation that all 63 pressurized tubes would burst) to minimize the temperature overshoot at the end of the test. Also, criterion (b), i.e., the high temperature limit, was established close to the expected burst temperature for the same reason. The test was terminated by the criterion (a) and all 63 pressurized tubes burst.

Quick-look Results

Quick-look data of interest are extensive and difficult to present in concise tabular format. Instead we have elected to display the data in a series of bundle layout diagrams and quick-look plots to facilitate visualization. It should be noted that these data are very preliminary and subject to change as detailed data tabulations and plots are generated from the magnetic data tape recorded during the test. In particular, burst temperatures, pressures, and times were read from quick-look data plots and they should be considered very approximate.

Superheated steam entered the array through the inlet nozzle, located on the north side of the bundle (see Fig. 1) at the 107-cm elevation, at a mass flux of 288 $g/s \cdot m^2$ which is equivalent to an initial Re of 140 at the top of the heated zone (91.5-cm elevation). Apparently this flow rate was so low that very little mixing took place as the steam entered and flowed downward through the bundle. Figure 6 shows the steam temperatures measured by each of the thermocouples about 0.5 s prior to power-on. As indicated by the measurements, the steam was cooled (losing heat to the rods) as it traversed the bundle from the inlet side (north) to the opposite (south) side, creating a gradient of about 24°C. The heat gained by the rods was conducted upward to the top of the vessel to be lost to the flange and to the external surroundings. The distribution was fairly constant (within 2°C) at the bottom of the heated zone as indicated in the figure.

The north-to-south skew in steam inlet temperature distribution was reflected in the initial temperature distribution of the fuel pin simulators at each of the instrumented elevations, although the extent of the skew decreased from top to bottom. Figures 7-10, show the distributions at elevations 84, 56, 20, and 5 cm (see Fig. 4 for relative positions). At the highest instrumented cross section (Fig. 7), there is gradient of 18-20°C across the bundle; the average temperature at this elevation was ~337°C. At the lowest instrumented cross section (Fig. 10), the gradient is 5-7°C, with an average of about 334°C. Figures 8 and 9 show consistent gradients and average temperatures between these extremes. The bundle

average temperature at each of the cross sections was very nearly the same, being only ~3°C lower at the bottom than at the top. However, comparison of Figs. 7 and 10 shows the rods on the north side had axial gradients of 10-12°C, while those on the south side had axial gradients of 2-3°C.

Attempts were made during the holdtime between the pretest power bump and the burst transient to correct the radial skew. These attempts were unsuccessful and it was decided to proceed with the test.

Eight thermocouples at the 38-cm elevation were selected and averaged electronically (in real time) to provide on-line monitoring of the bundle temperature as the test progressed. The thermocouples selected (all on interior simulators) are indicated in Fig. 11; the initial temperature measurements are also indicated. The data channel for the averaged data is identified (and plotted in a number of subsequent quick-look plots) as TAV-10.

Figure 12 shows the applied voltage and TAV-10 during the transient. This plot serves as a time mark for power-on and power-off. The average heating rate, as determined by TAV-10 from 15 to 50 s, is indicated with approximate temperature values determined from the plot. Figure 13 shows the pressure traces of the first and last tubes to burst. Approximate times of burst for all the pressurized tubes are indicated in Fig. 14. A frequency plot of the burst times is shown in Fig. 15. Initial and approximate burst pressures are given in Fig. 16. Approximate measured burst temperatures (as read from quick-look plots) and burst temperatures calculated for a heating rate of 10 K/s, using the correlation developed from our single rod tests, are indicated in Fig. 17. The burst data are plotted and compared to correlation predictions (using the measured burst pressure) in Fig. 18. In general, the exterior rods burst at higher pressures than did the interior rods. This probably indicates more uniform temperatures and greater deformation for the interior rods.

As the tubes burst, the vessel (steam) pressure outside the tubes increased significantly, due to escaping pressurizing gas within the simulators, as indicated in Fig. 19. A plot of the inlet steam temperature, as measured by the three thermocouples at the top of the bundle (see Fig.

5 for locations), is shown in Fig. 20. Similarly, steam outlet temperature measurements are shown in Fig. 21. Both these figures show significant temperature perturbations during the time bursts were occurring. The increase in inlet temperature is the result of reverse flow.

Although the thin shroud was not heated electrically, its temperature increased significantly during the transient as shown in Fig. 22. The step increases at a scan time of ~55 s are attributed to escaping hot gases. The mechanisms of heat transfer causing the shroud temperature increase during the transient have not yet been identified. Possible mechanisms include radiation losses from the bundle and steam (although the shroud was gold plated to give a highly reflective surface) and convective losses from the steam.

As indicated earlier, external thermocouples were attached to four simulators (see Fig. 3) to obtain azimuthal temperature gradients during the test. Results of the measurements on simulator 28 are plotted in Fig. 23. Results from an internal thermocouple at the same elevation are also shown. Obviously the inside temperature must be higher than the outside temperature and the fact that the data show the opposite is erroneous. This obvious inconsistency is likely due to internal (within the computer) conversion of the raw data signals from the type S external thermocouples to engineering units for producing the quick-look plots. The importance of the graph is related to the external thermocouple measurements. As shown, very small gradients existed prior to the onset of deformation (which corresponds to the point where pressure begins to decrease), then as deformation increased, measureable gradients developed. At a scan time of 52.5 s from power-on (the only time for which a data tabulation is presently available), the gradient was 10.5°C. By the time of burst the gradient had increased to about 20°C, as estimated from the graph.

Bundle Deformation

Following the burst test the bundle was removed from the vessel. After certain instrumentation checks were made, the north shroud face was

removed for initial observation. Figures 24 and 25 show pretest and posttest views for comparison. The location of the heated portion can be noted by the deformation observed in Fig. 25 and from the schematic of Fig. 1. When this photograph and the ones following are compared to those of B-3, deformation appears to be at least as great as in B-3. However, it is impossible to make any but qualitative observations of the extent of deformation until the flow tests and sectioning are complete.

The remaining shroud faces were next removed and photographs (see Figs. 26 through 29) were taken showing the four faces of the bundle. The upper three grids are shown in these figures with the uppermost grid no. 3 (steam inlet end) located outside of the heated zone. Extensive deformation (and bursts) can be noted in the area just above grid no. 2 although calculations had indicated that, with the same steam mass flux and other test parameters matching those of B-3, the bursts would be expected to occur between grids 1 and 2. The effect on deformation of the temperature skew (discussed earlier) from north to south can be noted in Figs. 26 and 28. In the area between grids 3 and 2, the area with the most pronounced temperature skew, it can be noted that the north face sustained the greater amount of deformation. Perhaps the most revealing illustration of the effect of this temperature skew on deformation can be noted in Fig. 27 of the east face. Diminishing deformation can be observed as the bundle is traversed from the north face to the south face between grids 3 and 2.

Further disassembly was necessary both to determine burst locations and in preparation for flow testing. The simulator upper and lower seal glands were removed successfully but the removal of the internal heaters was not completely successful. Many of the heaters were difficult to remove by ordinary means and eleven were impossible. It was decided that extraordinary force, which might result in the distortion of the deformed tubes, should not be used. Therefore eleven fuel pin simulators still contain internal heaters which prevent determination of the exact burst locations until the bundle is sectioned after the water flow tests. Burst locations for the tubes without heaters were obtained by use of a borescope. The approximate burst locations of the tubes containing heaters

were determined by observing the exit point of injected smoke. The borescope measurement provides a fairly accurate axial position but the orientation is only approximate. Where possible the bursts are described by elevation, orientation, and length in Table 1.

Two of the simulators (Nos. 7 and 53) apparently sustained pin hole type openings which occurred at or near internal thermocouples attachment locations. Where extensive tube-wall thinning occurred, it is not unreasonable to expect that small surface perturbations, such as caused by a thermocouple attachment, could determine the failure point.

The burst information of Table 1 is provided in a graphical manner by Figs. 30 and 31. As would be expected from the earlier discussion of the north-to-south temperature skew, a predominance of high burst elevations can be noted for the first two rows of tubes (i.e., simulators 1 through 16 in Fig. 31) beginning from the north face.

Table 2 contains a tabulation of the axial shrinkage of individual simulators. In comparison with B-3 it will be noted that 2.9% is the maximum shrinkage in both bundles although the average shrinkage is slightly higher in B-5. Table 3 lists the average shrinkage of the 63 pressurized simulators and the resultant relocation of grids.

Table 1. Approximate burst locations in B-5

Simulator No.	Approximate burst location		Approximate burst length (cm)
	Axial[a] (cm)	Angle[b] (deg)	
1	73.4	110	1.6
2	75.6	120	3.0
3	24.9	240	1.8
4	77.7	180	2.4
5	78.0	200	1.6
6	72.5	120	1.9
7	74.1	70	0[d]
8	79.1	180	3.1
9	75.2	70	2.3
10	20.4	50	2.0
11	32.8	310	2.5
12	72.9	50	1.7
13	74.2	130	3.9
14	74.6	60	2.2
15	76[c]	[c]	[c]
16	74.4	360	2.9
17	54[c]	[c]	[c]
18	26.4	20	2.1
19	39.7	240	2.5
20	28.9	60	2.4
21	73.5	60	2.0
22	54[c]	[c]	[c]
23	50.5	200	2.6
24	21.3	310	1.7
25	15.7	60	1.7
26	20.6	40	2.0
27	46[c]	[c]	[c]
28	72.9	60	2.2
29	17[c]	[c]	[c]
30	48.7	160	3.2
31	45.2	230	2.5
32	37.1	240	2.0
33	15.6	140	1.3
34	46[c]	[c]	[c]
35	22.1	40	2.8
36	44[c]	[c]	[c]
37	75.0	60	2.1
38	17.2	70	1.9
39	21.0	70	1.5
40	70.6	330	1.9
41	16.2	90	3.5
42	18.8	30	3.8

Table 1. Continued

Simulator No.	Approximate burst location		Approximate burst length (cm)
	Axial[a] (cm)	Angle[b] (deg)	
43	39[c]	[c]	[c]
44	45[c]	[c]	[c]
45	74.0	70	2.0
46	22.9	160	4.3
47	49.8	160	2.3
48	46.9	220	2.0
49	16.8	70	2.1
50	20.9	60	2.6
51	17.9	70	2.3
52	33.2	240	2.7
53	46.3	80	0[d]
54	20.2	60	2.5
55	23.4	340	2.8
56	71.3	330	1.4
57	19.3	20	2.3
58	19.5	50	2.3
59	54[c]	[c]	[c]
60	33.4	50	2.6
61	35[c]	[c]	[c]
62	[e]	[e]	[e]
63	34.3	250	3.3
64	17.0	330	1.8

[a]Elevation above bottom of heated zone.

[b]Measured clockwise looking down on top of bundle.

[c]Internal heater could not be removed. Burst location was determined only approximately by observing exit point of injected smoke. This technique does not give orientation and length of burst.

[d]Pin hole opening probably at thermocouple attachment.

[e]Tube unpressurized.

Table 2. Approximate axial shrinkage of individual tubes in B-5 test

Simulator No.	Heated length change	
	cm	%
1	1.5	1.6
2	2.3	2.5
3	2.3	2.5
4	1.9	2.1
5	2.3	2.5
6	2.3	2.6
7	2.2	2.4
8	2.1	2.3
9	2.3	2.6
10	2.4	2.6
11	2.3	2.5
12	2.3	2.6
13	2.3	2.5
14	2.3	2.5
15	2.3	2.6
16	1.6	1.8
17	2.2	2.4
18	1.9	2.1
19	2.7	2.9
20	2.3	2.6
21	1.6	1.8
22	2.7	2.9
23	2.3	2.5
24	2.2	2.4
25	2.3	2.5
26	2.2	2.4
27	2.2	2.4
28	2.4	2.6
29	2.2	2.4
30	2.3	2.6
31	2.0	2.2
32	2.2	2.4
33	2.3	2.5
34	2.3	2.6
35	2.3	2.6
36	2.6	2.8
37	2.4	2.6
38	2.5	2.7
39	2.5	2.7
40	2.2	2.4
41	2.3	2.6
42	2.6	2.8

Table 2. Continued

Simulator No.	Heated length change	
	cm	%
43	2.0	2.2
44	2.5	2.7
45	2.5	2.8
46	2.5	2.7
47	2.3	2.6
48	2.3	2.5
49	2.0	2.2
50	1.6	1.8
51	2.4	2.6
52	2.3	2.5
53	2.5	2.7
54	2.3	2.6
55	2.3	2.5
56	2.3	2.5
57	2.3	2.6
58	2.1	2.3
59	2.1	2.3
60	2.1	2.3
61	2.2	2.4
62	0[a]	0[a]
63	2.3	2.6
64	1.8	2.0

[a]Simulator No. 62 was unpressurized.

Table 3. Overall axial shrinkage of bundle B-5 as reflected by relocation of grids and bottom of heated zone

Position	Change in elevation (cm)	Heated length above this position (cm)	Axial shrinkage (%)
Lower heated zone	2.2 ± 0.25[a]	91.4	2.4
Grid #1	2.0	81.2	2.5
Grid #2	0.6	25.3	2.4

[a]This represents the average of 63 simulators (No. 62 was unpressurized).

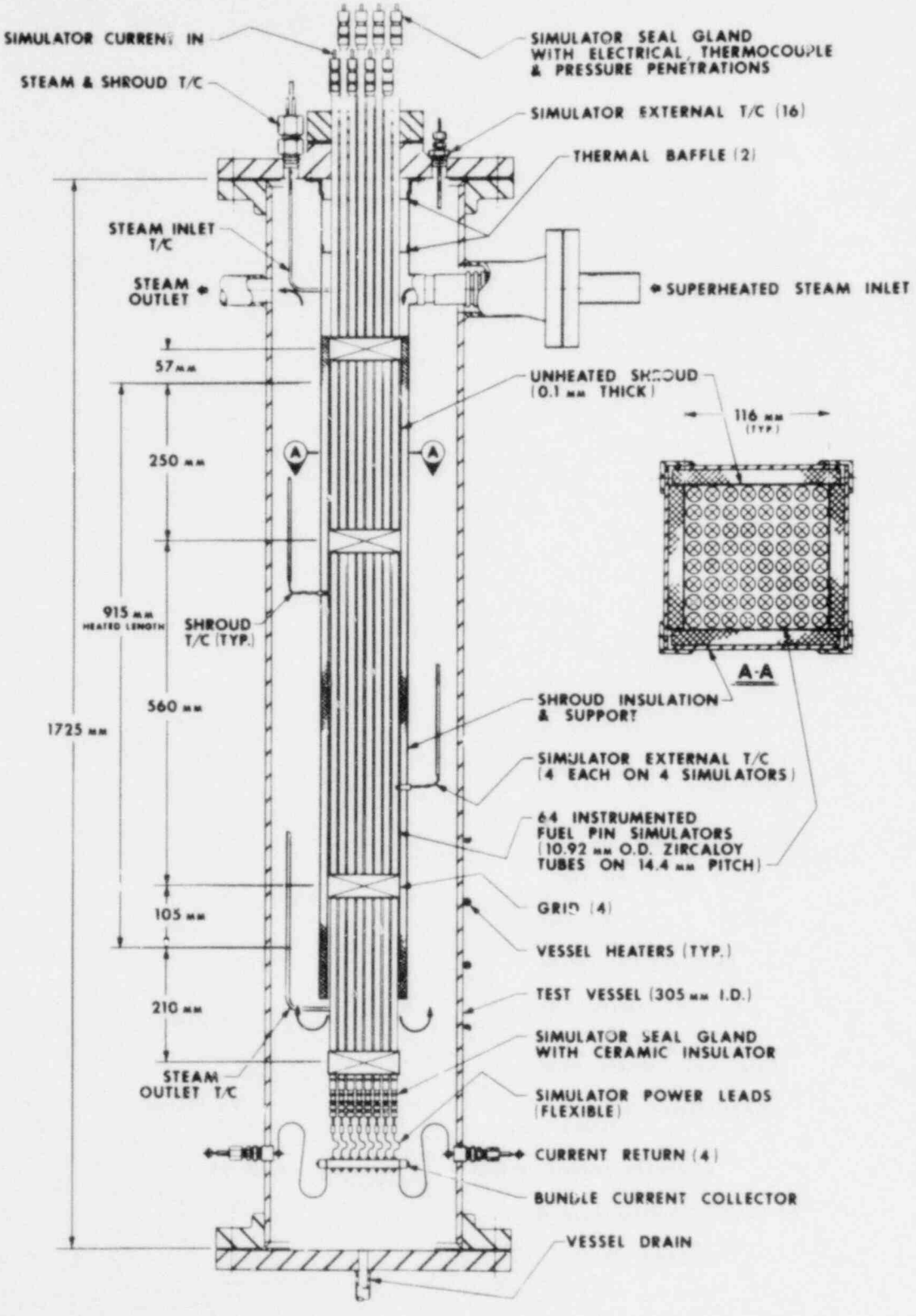

Fig. 1. Schematic of B-5 (8 × 8) bundle test assembly.

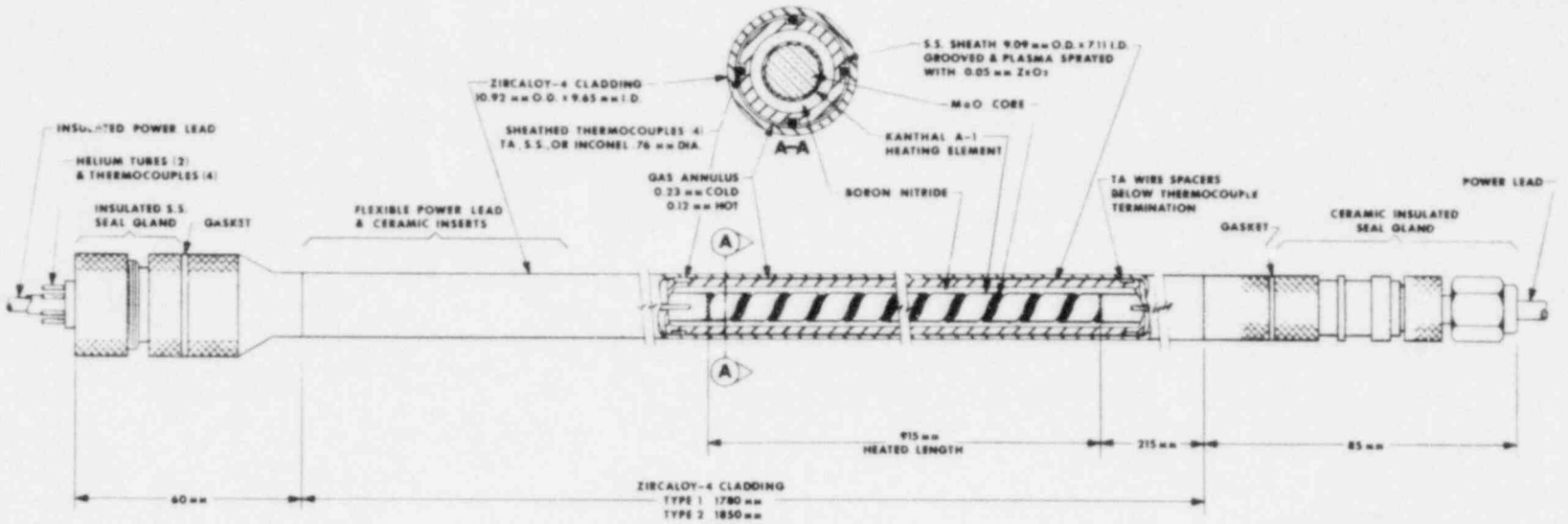

Fig. 2. MRBT Fuel Pin Simulator.

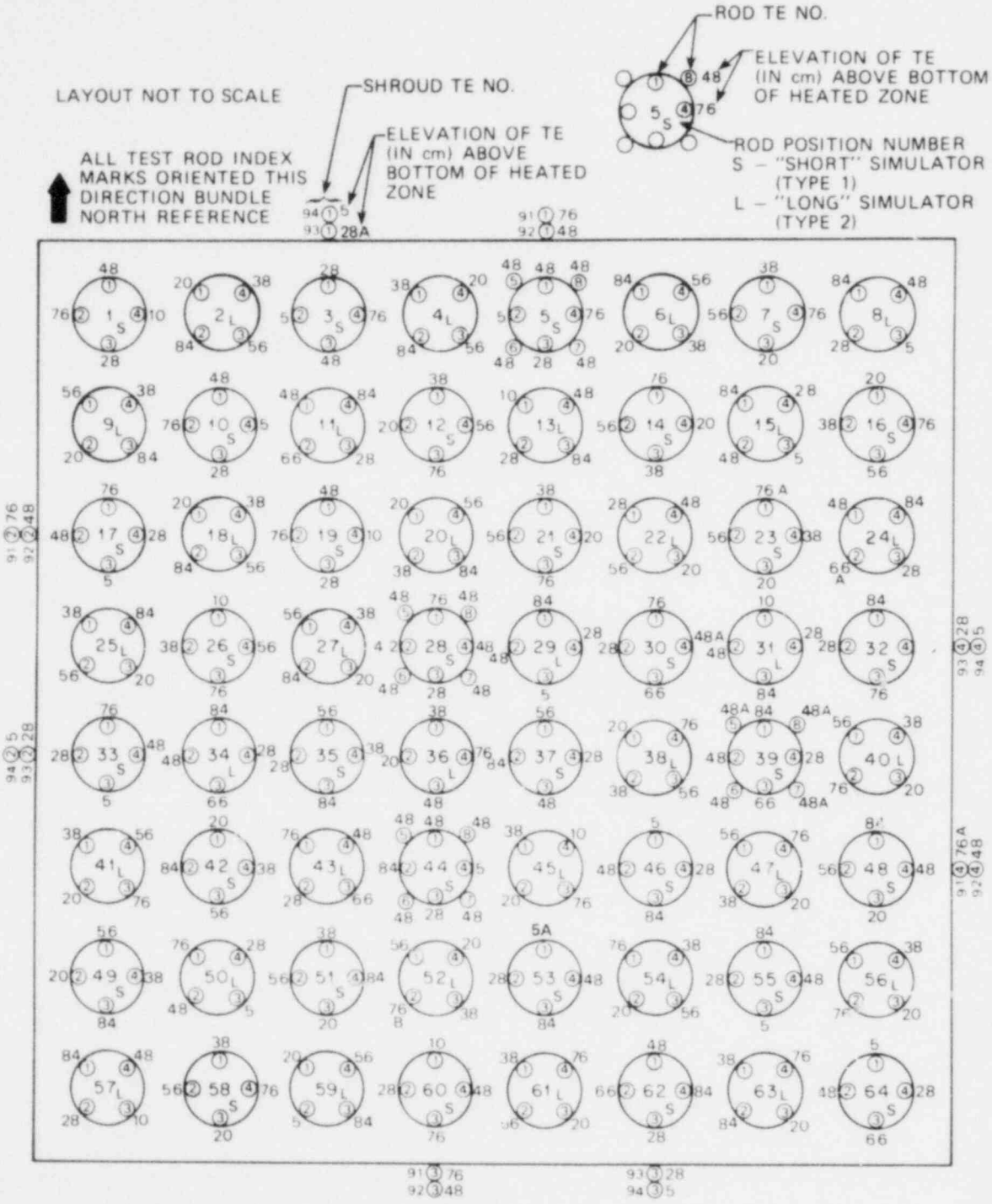

NOTES:

A. BECAME DETACHED DURING ASSEMBLY.
B. JUNCTION BECAME GROUNDED AFTER ASSEMBLY.

Fig. 3. As-built thermocouple locations in B-5 test (plan view).

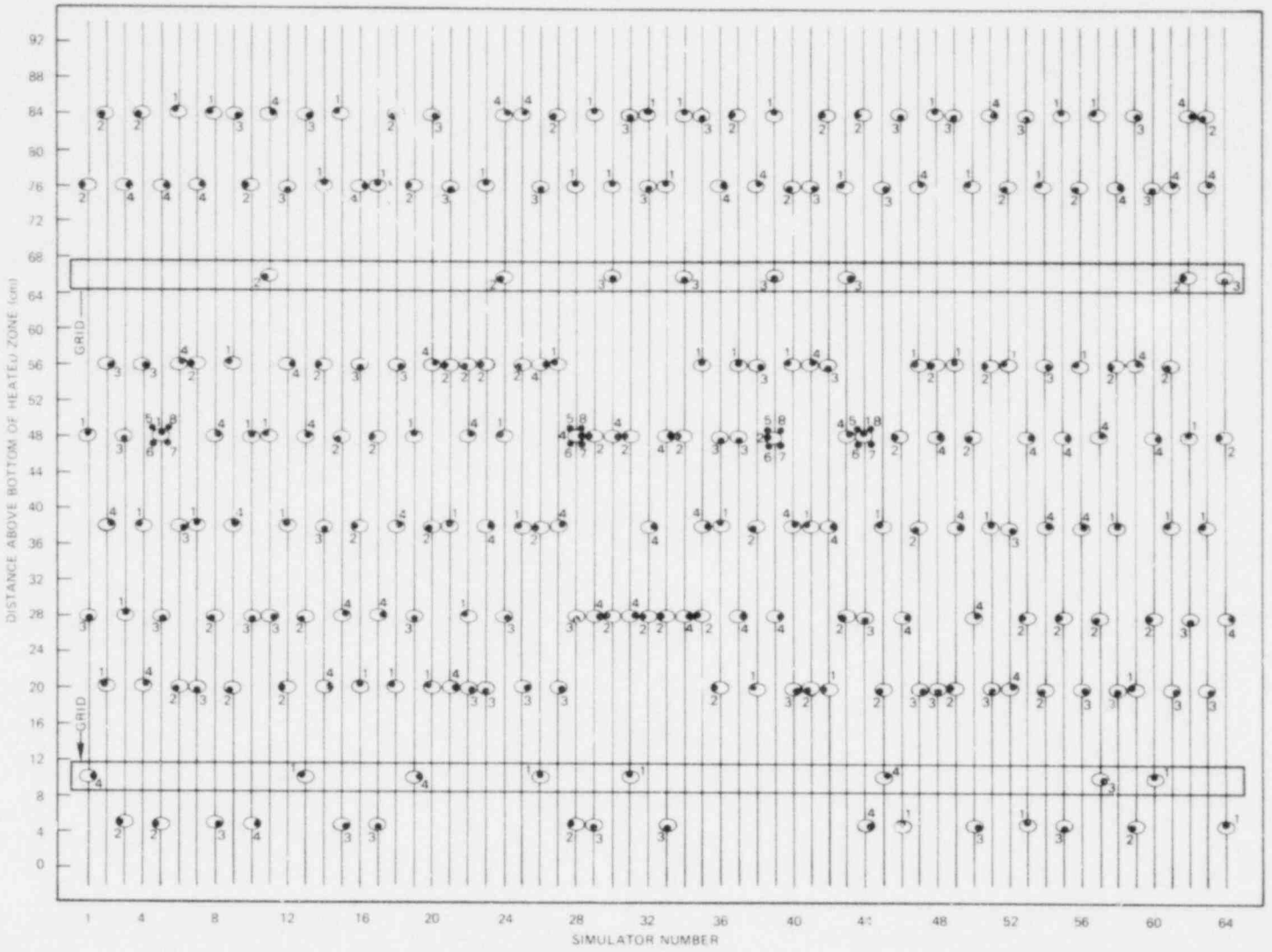

Fig. 4. As-built thermocouple locations in B-5 test (elevation view).

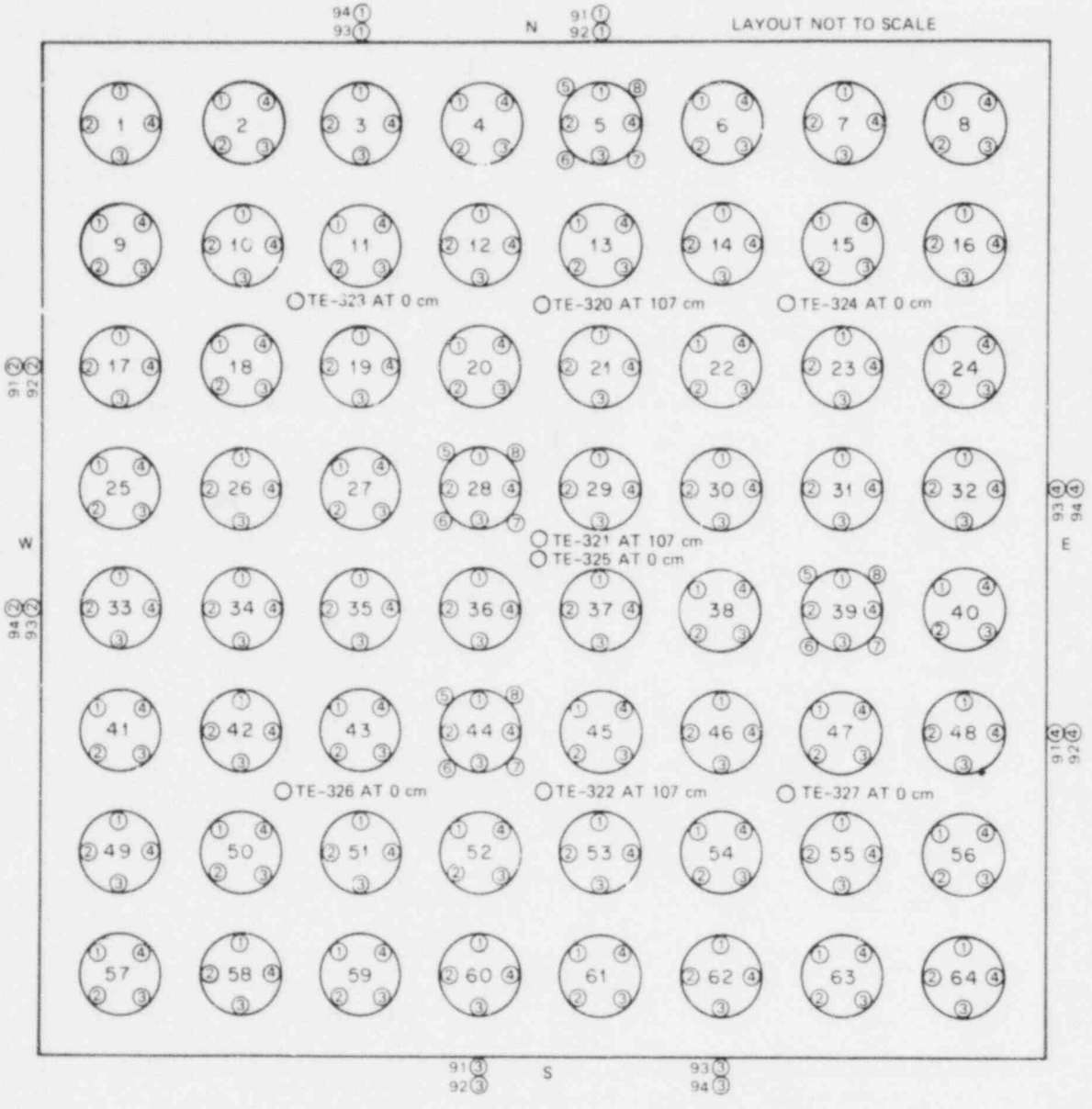

Fig. 5. Steam thermocouple identifications and locations in B-5 test. Elevations are in centimeters above bottom of heated zone.

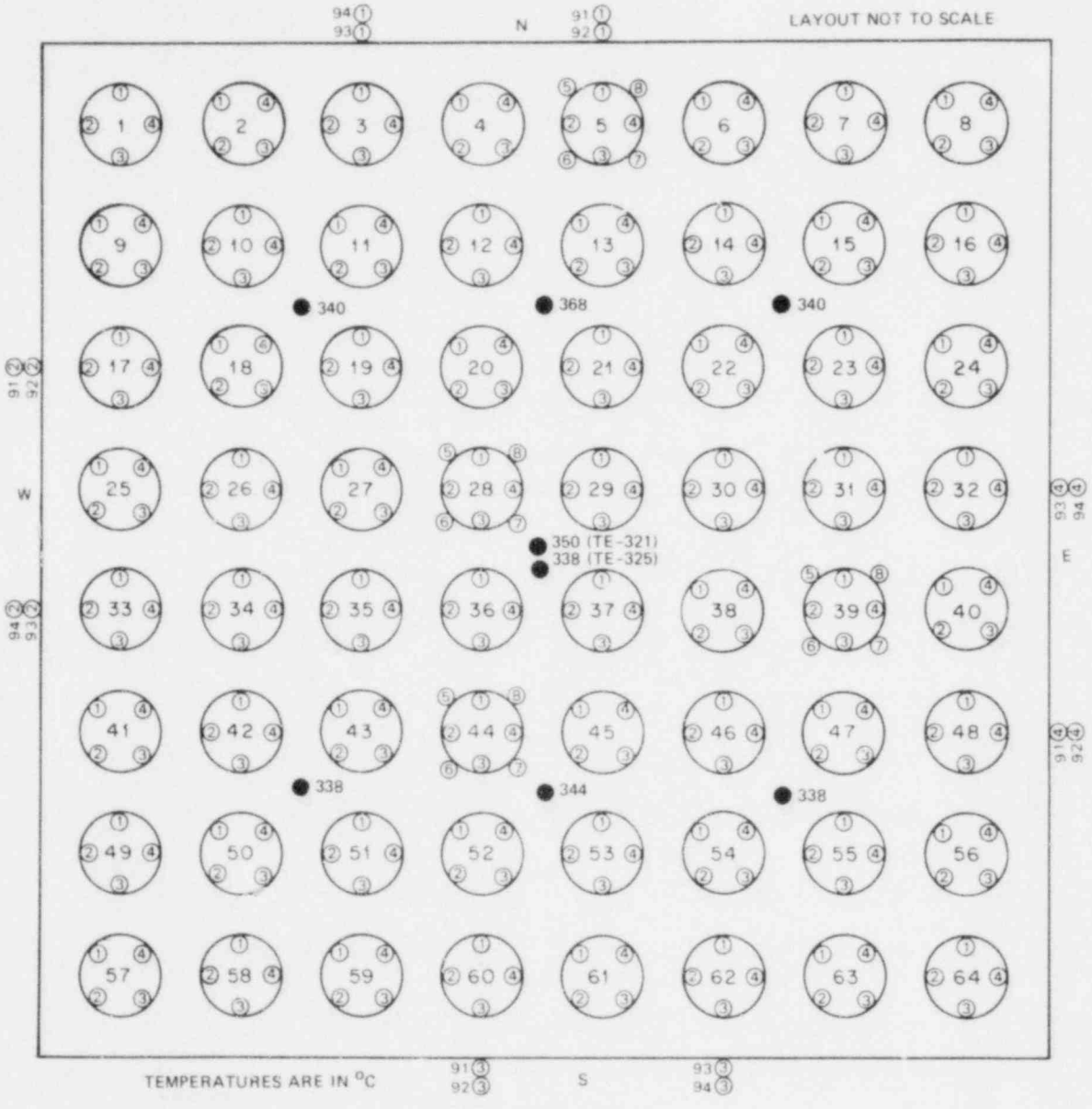

Fig. 6. Steam temperatures in B-5 test prior to power-on.

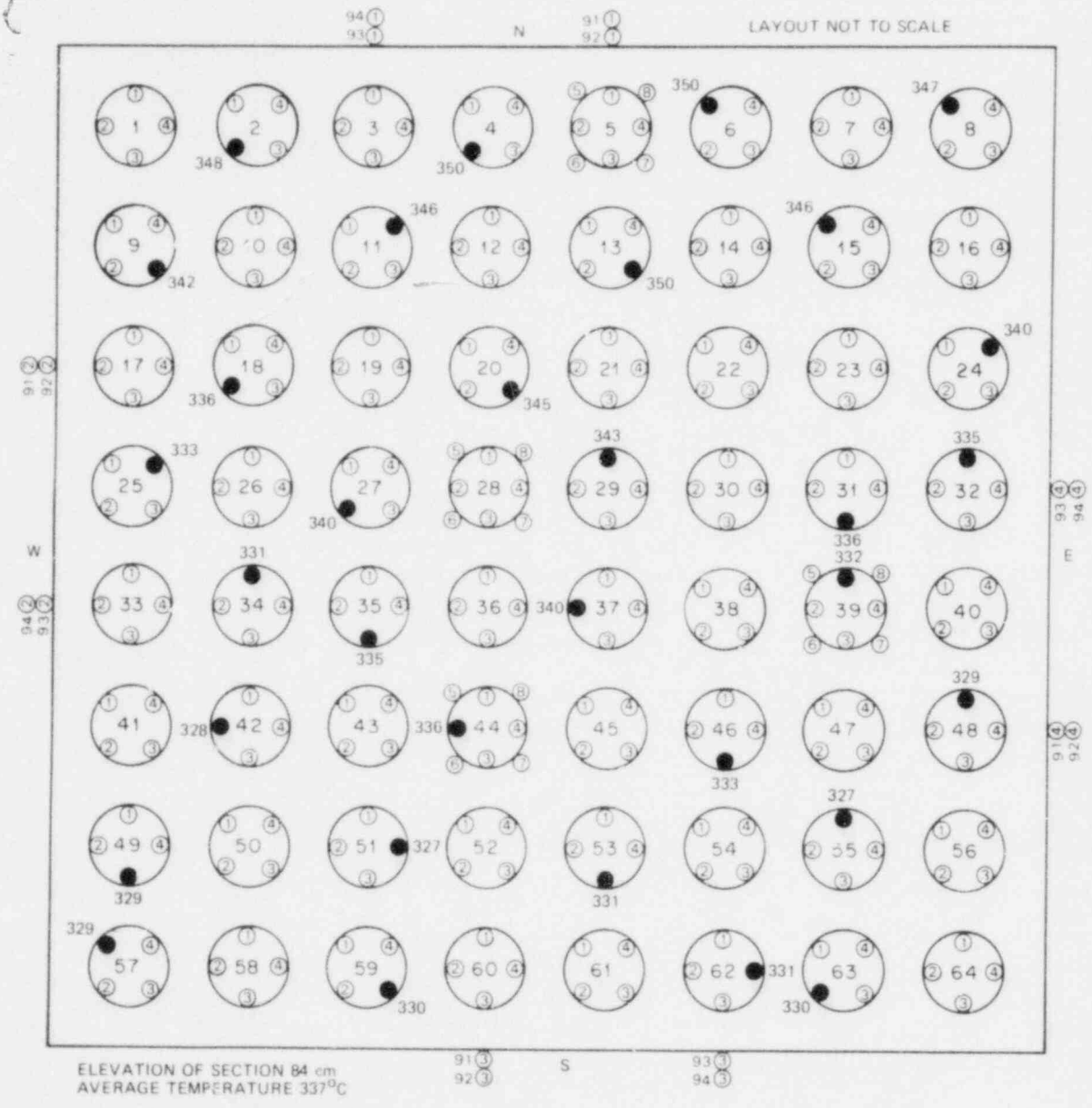

Fig. 7. Initial radial temperature distribution at 84-cm elevation.

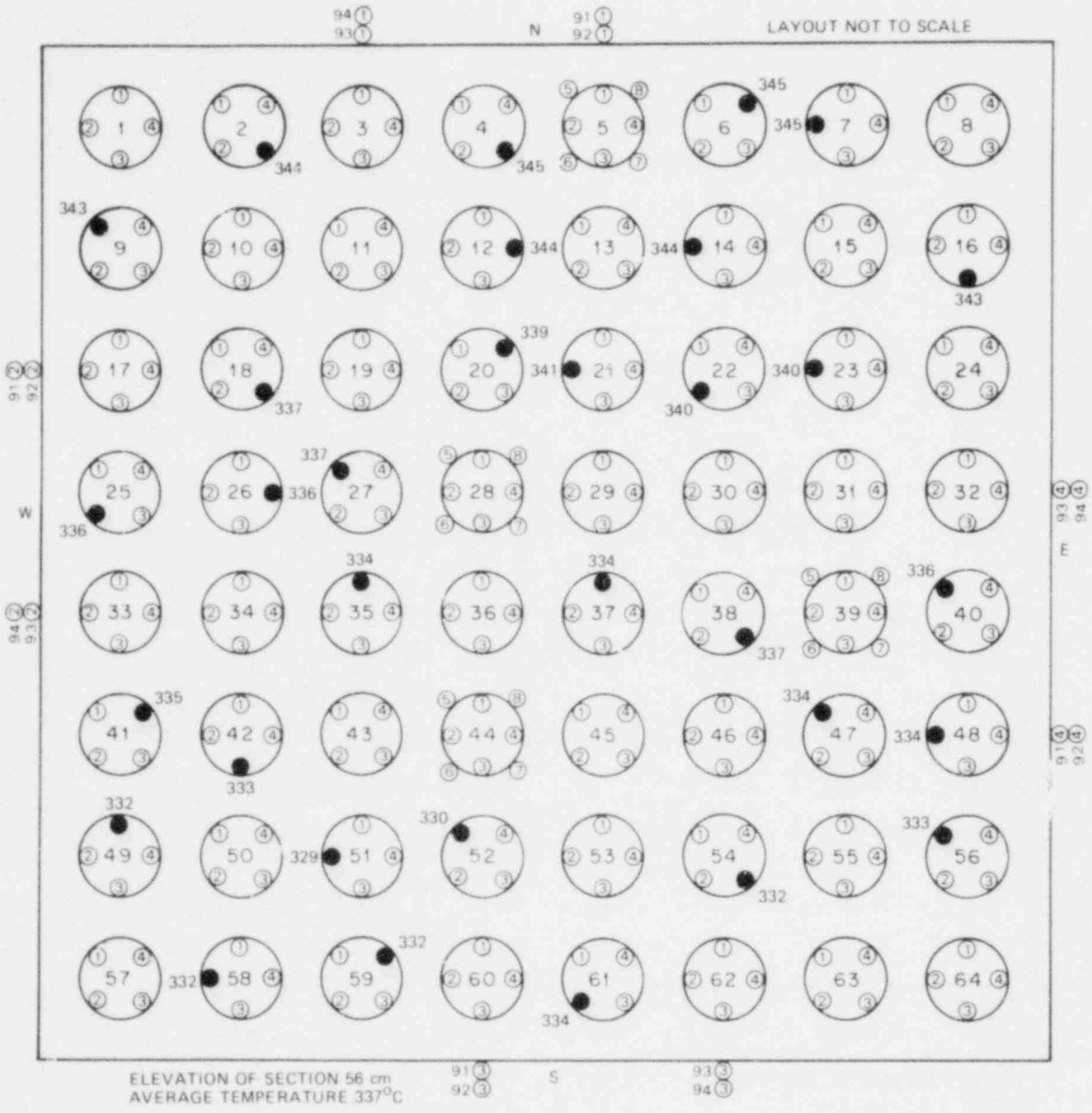

Fig. 8. Initial radial temperature distribution at 56-cm elevation.

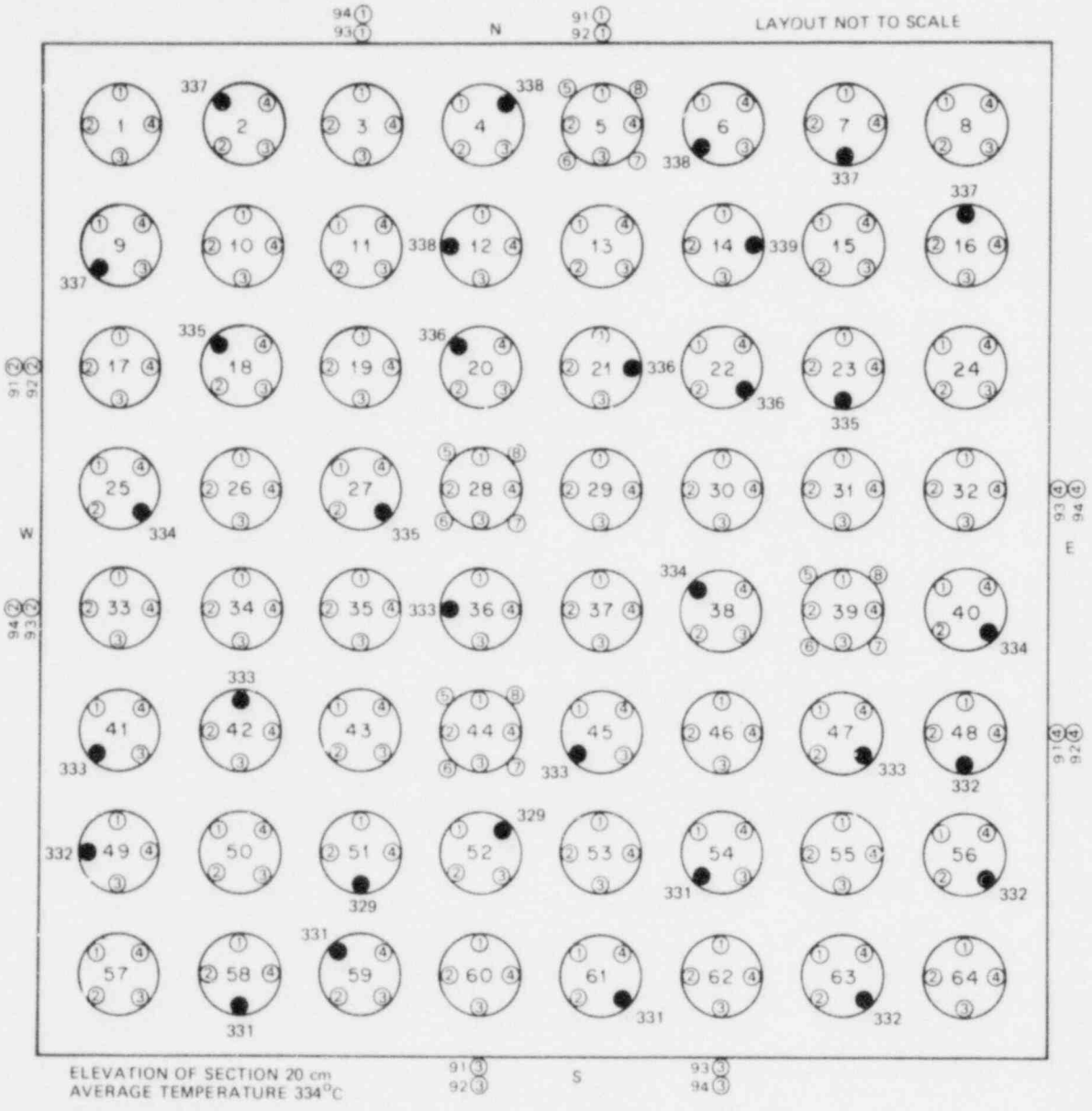

Fig. 9. Initial radial temperature distribution at 20-cm elevation.

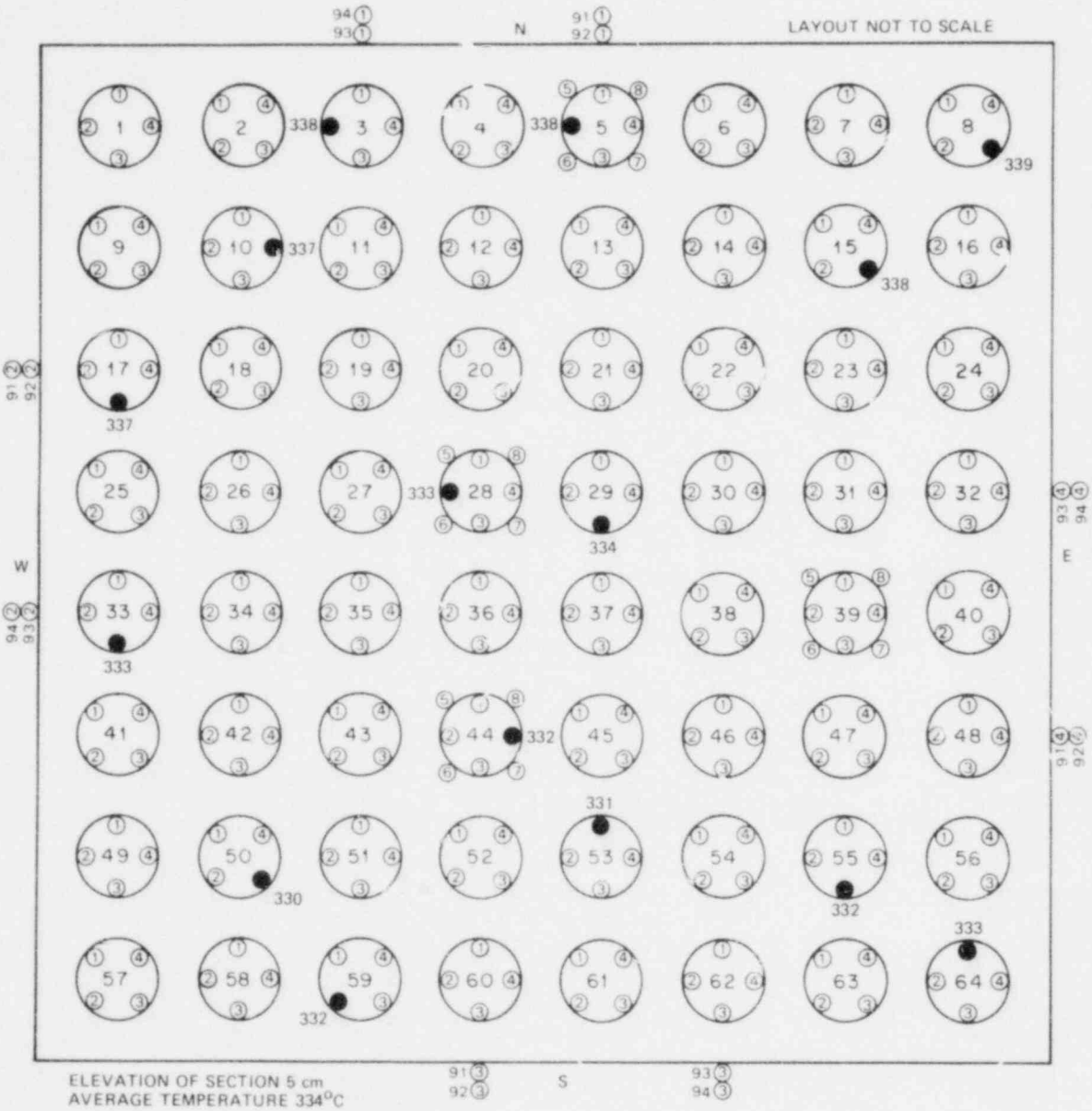

Fig. 10. Initial radial temperature distribution at 5-cm elevation.

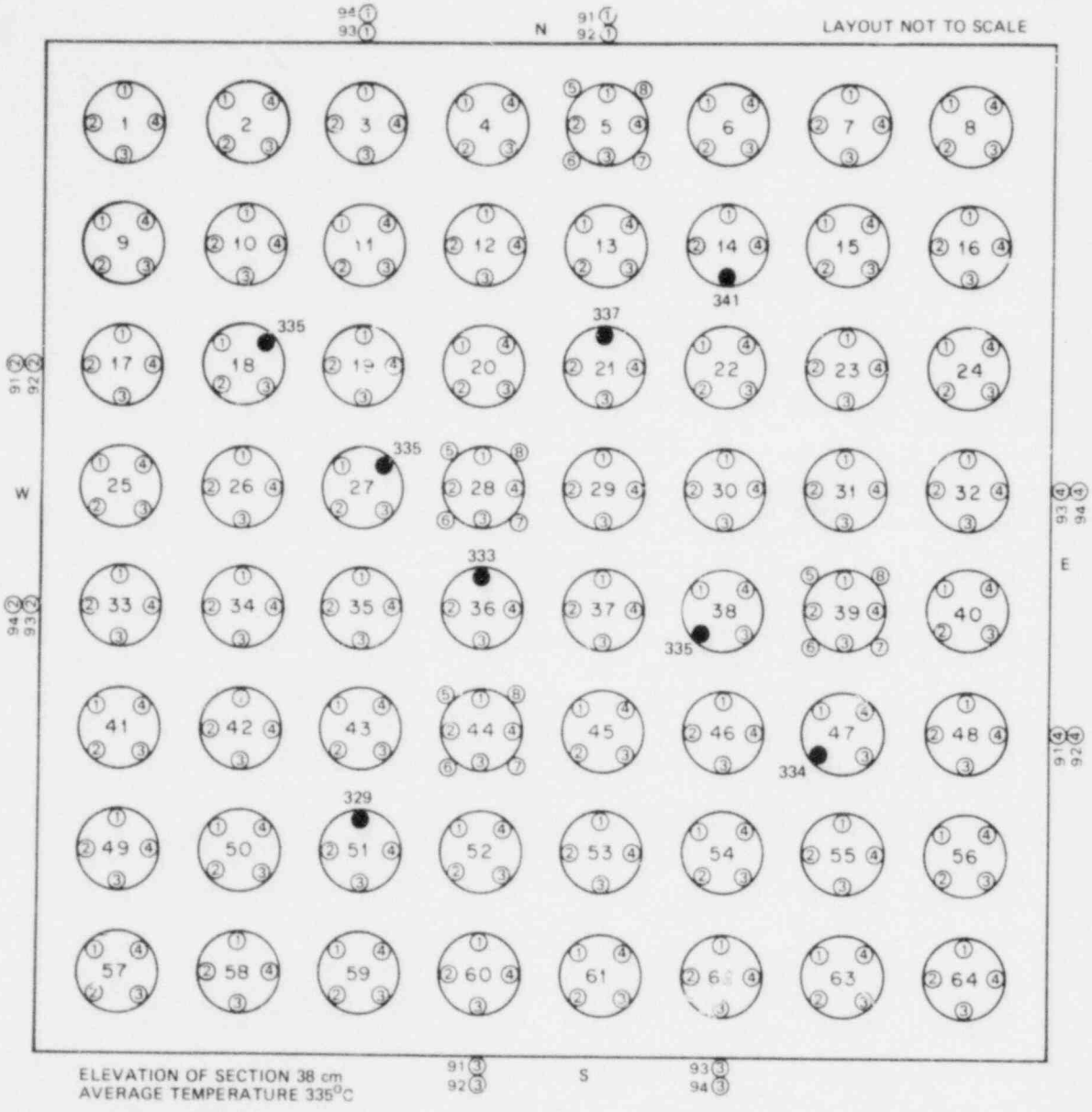

Fig. 11. Locations and initial temperatures of TEs used for average temperature data channel TVA-10.

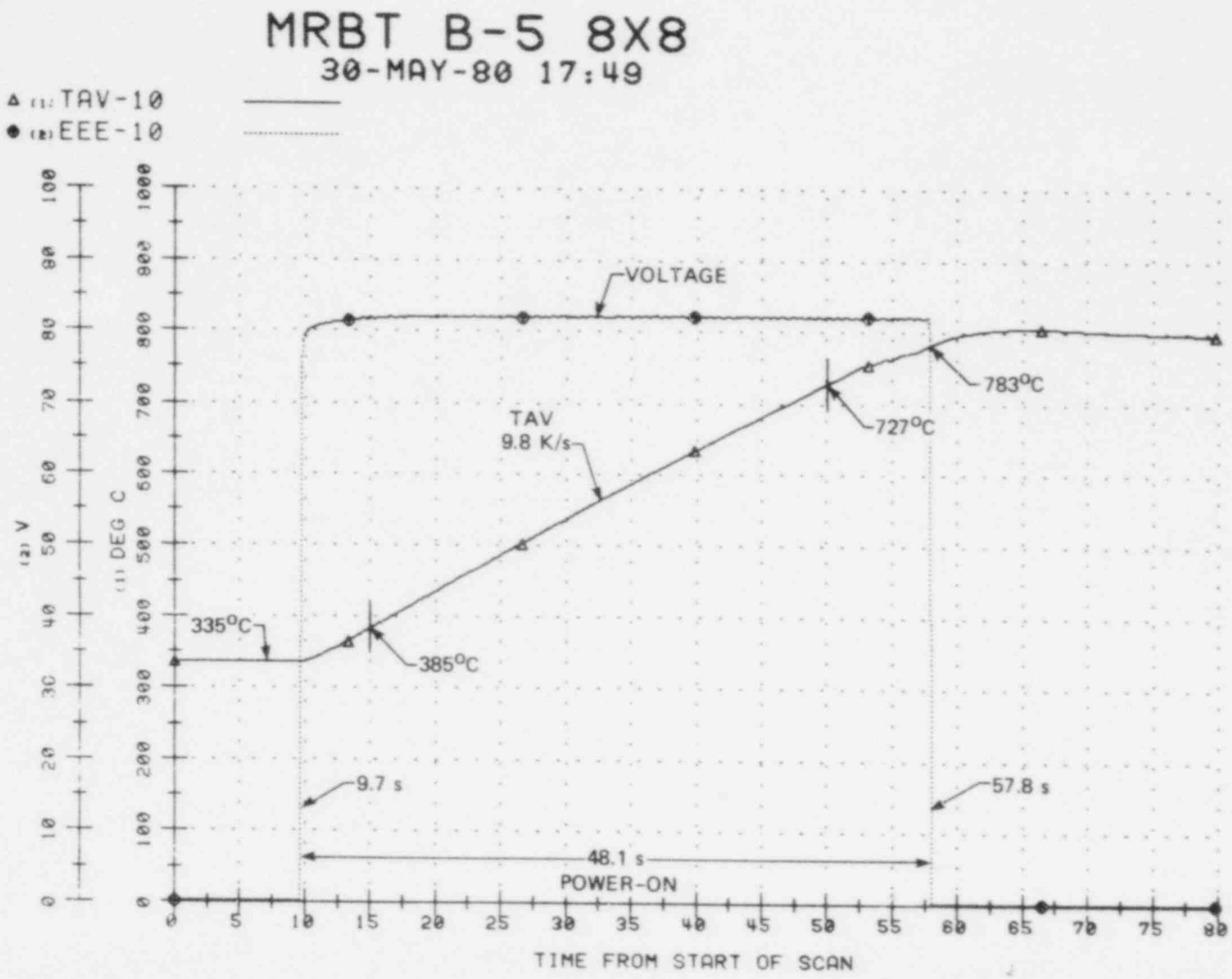

Fig. 12. Applied voltage and TAV-10 during B-5 test.

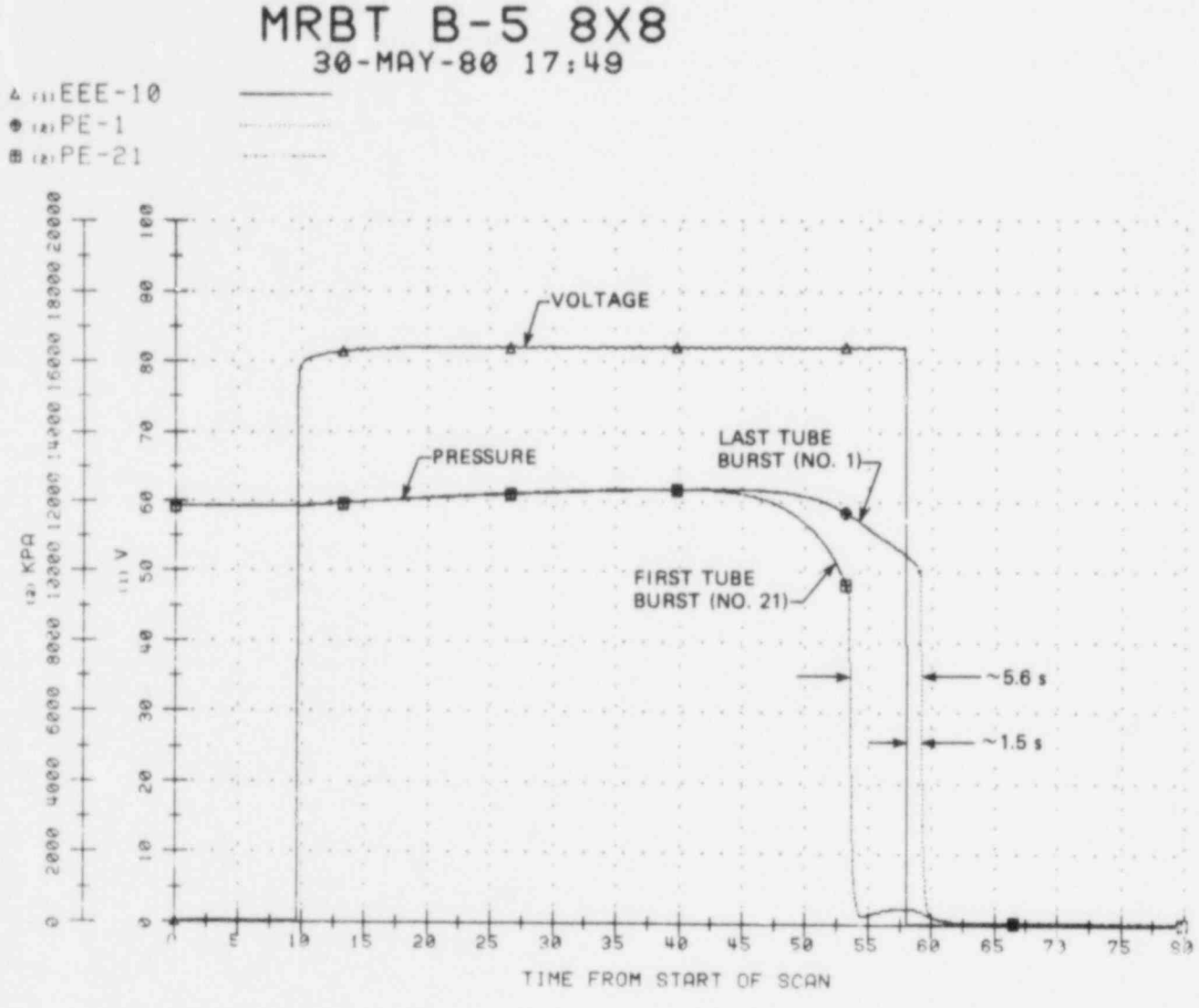

Fig. 13. Pressure plots of first and last tube bursts.

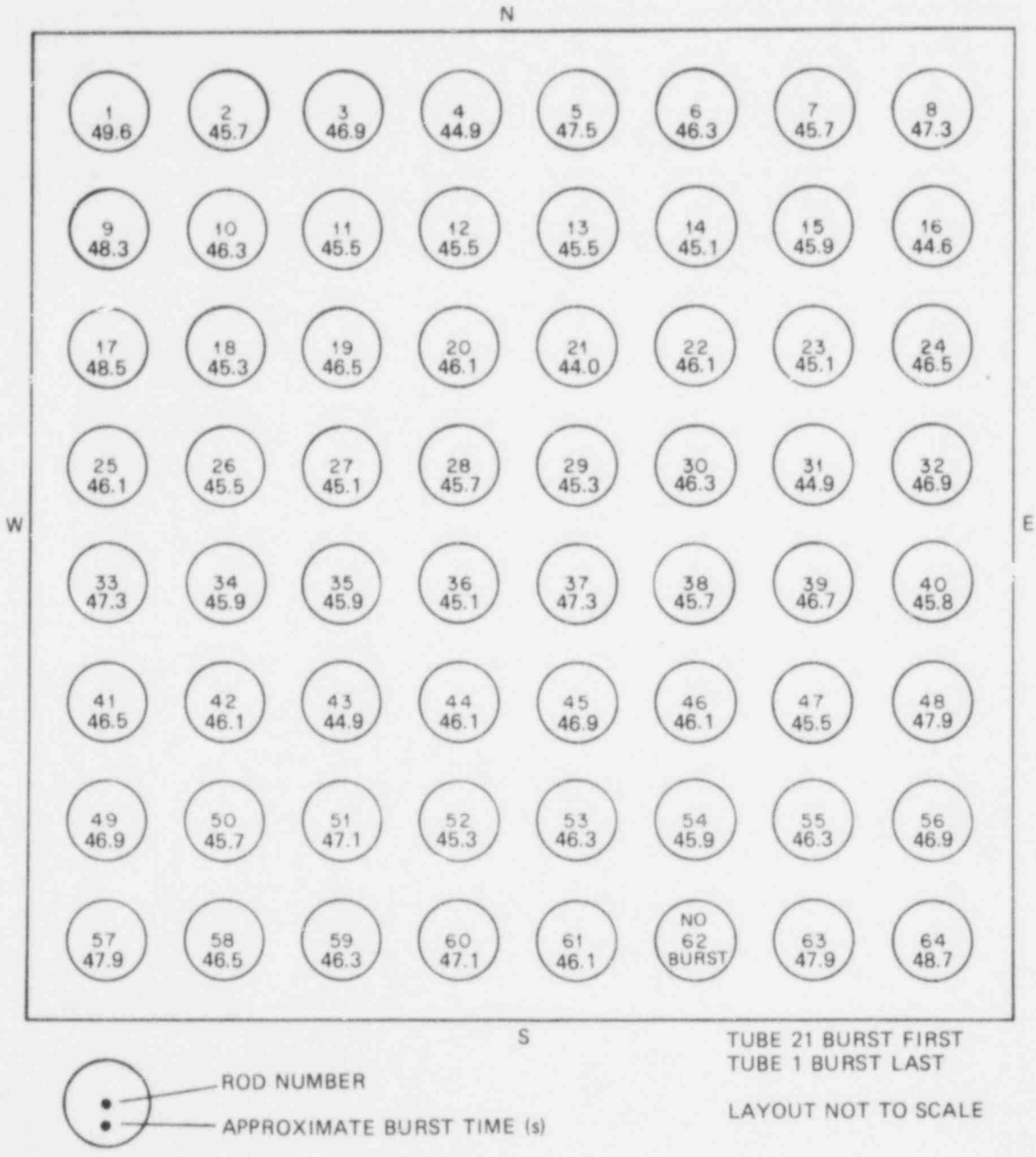

Fig. 14. Approximate burst times.

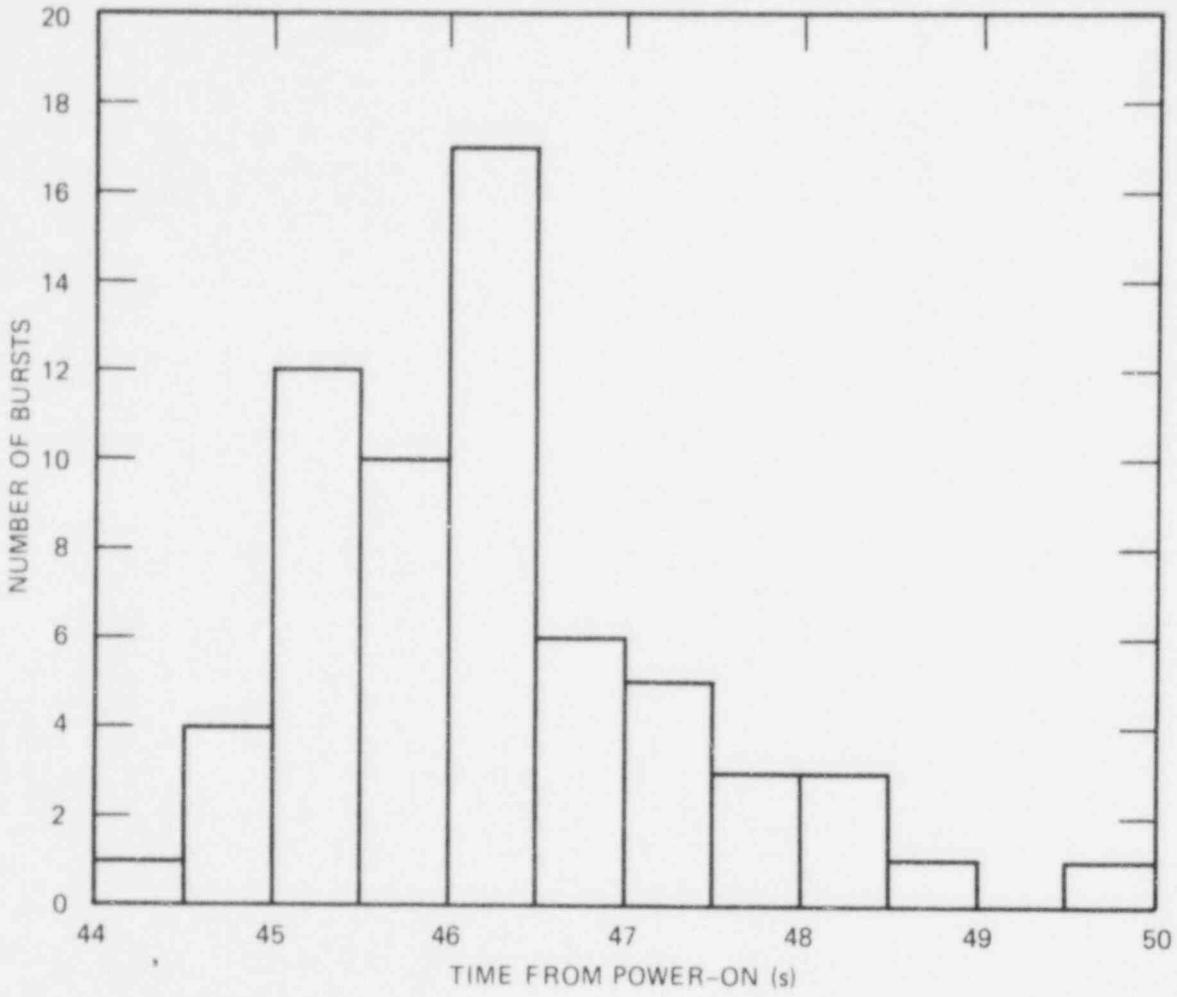

Fig. 15. Approximate burst frequency.

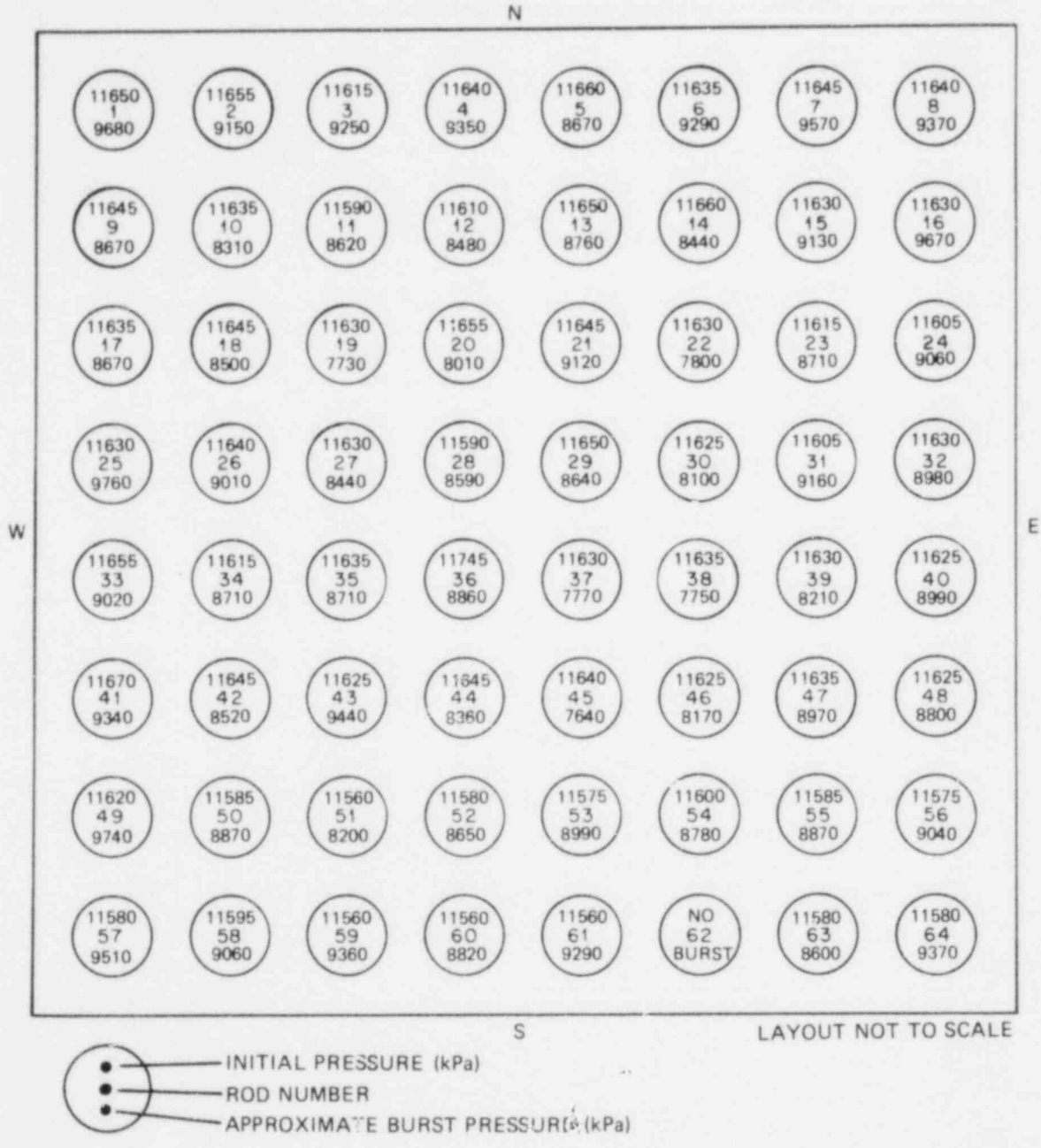

Fig. 16. Initial and approximate burst pressures.

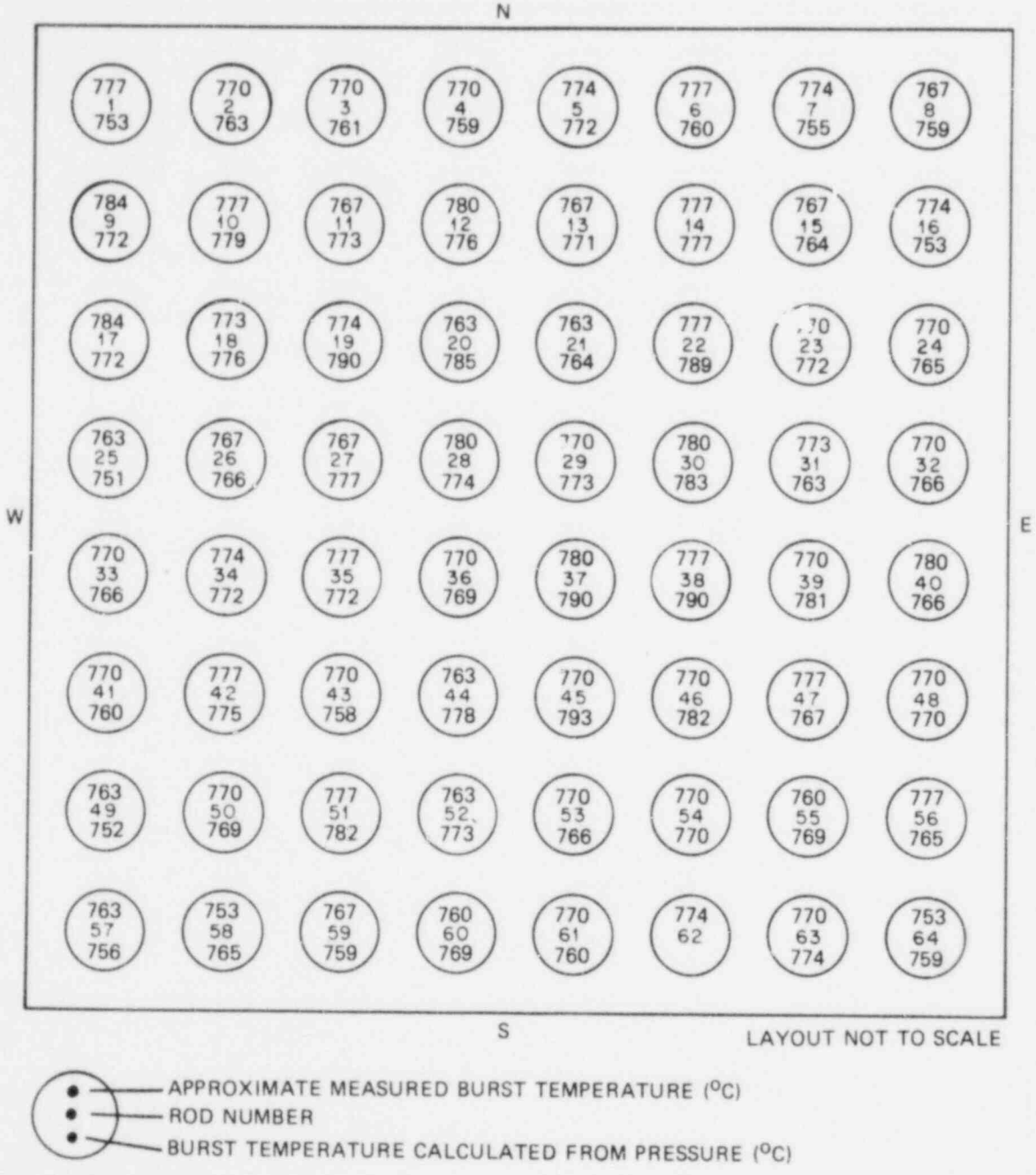

Fig. 17. Approximate burst temperatures.

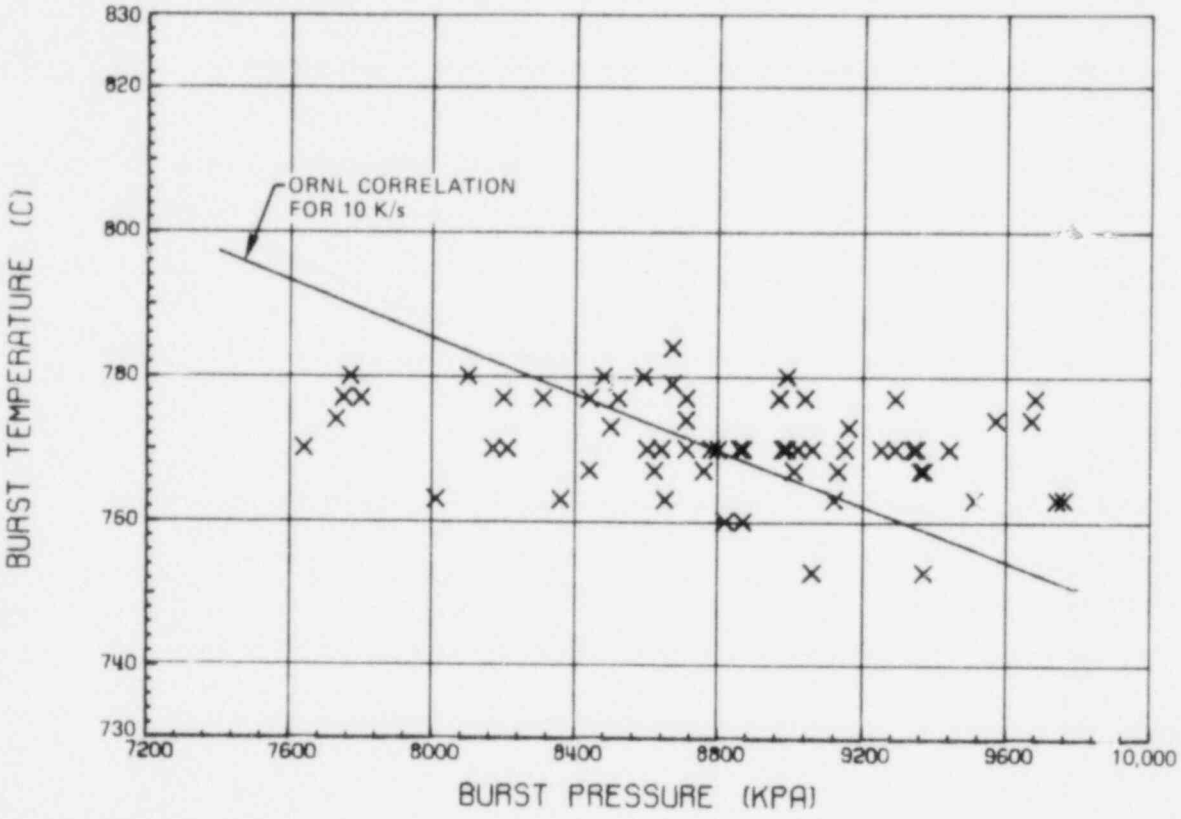

Fig. 18. Comparison of B-5 experimental data with burst temperature predicted by correlation using measured burst pressure.

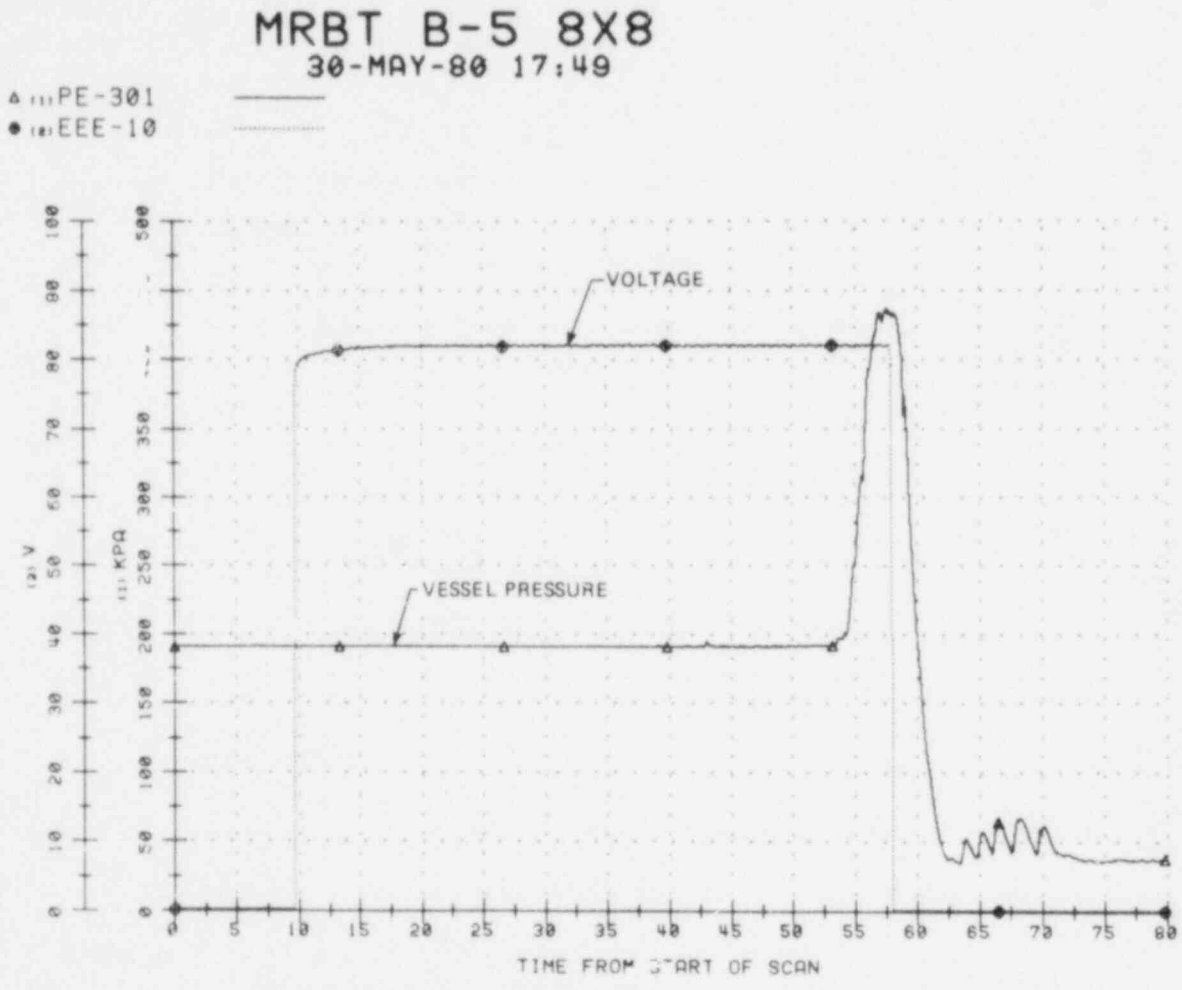

Fig. 19. Steam pressure during transient.

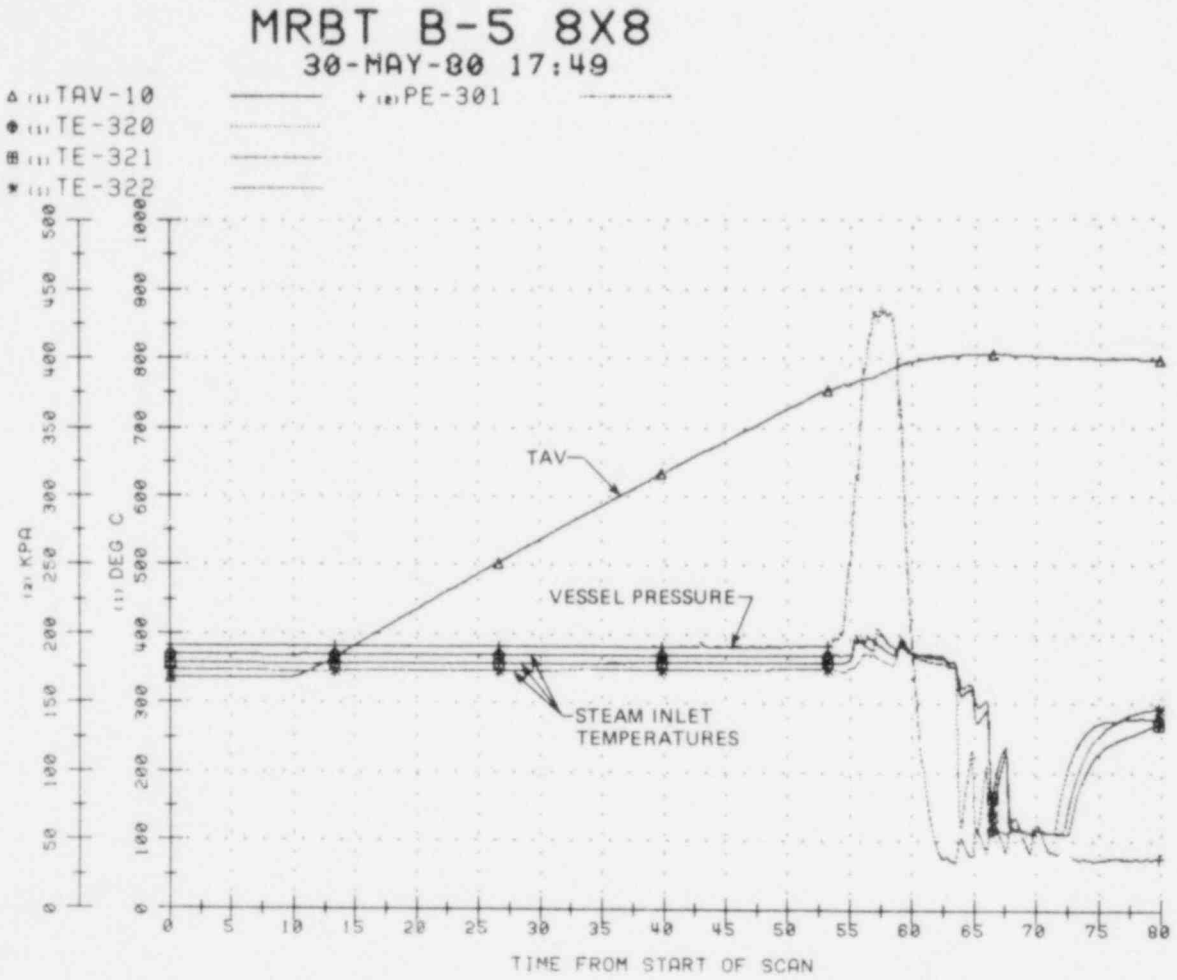

Fig. 20. Steam inlet temperature during test.

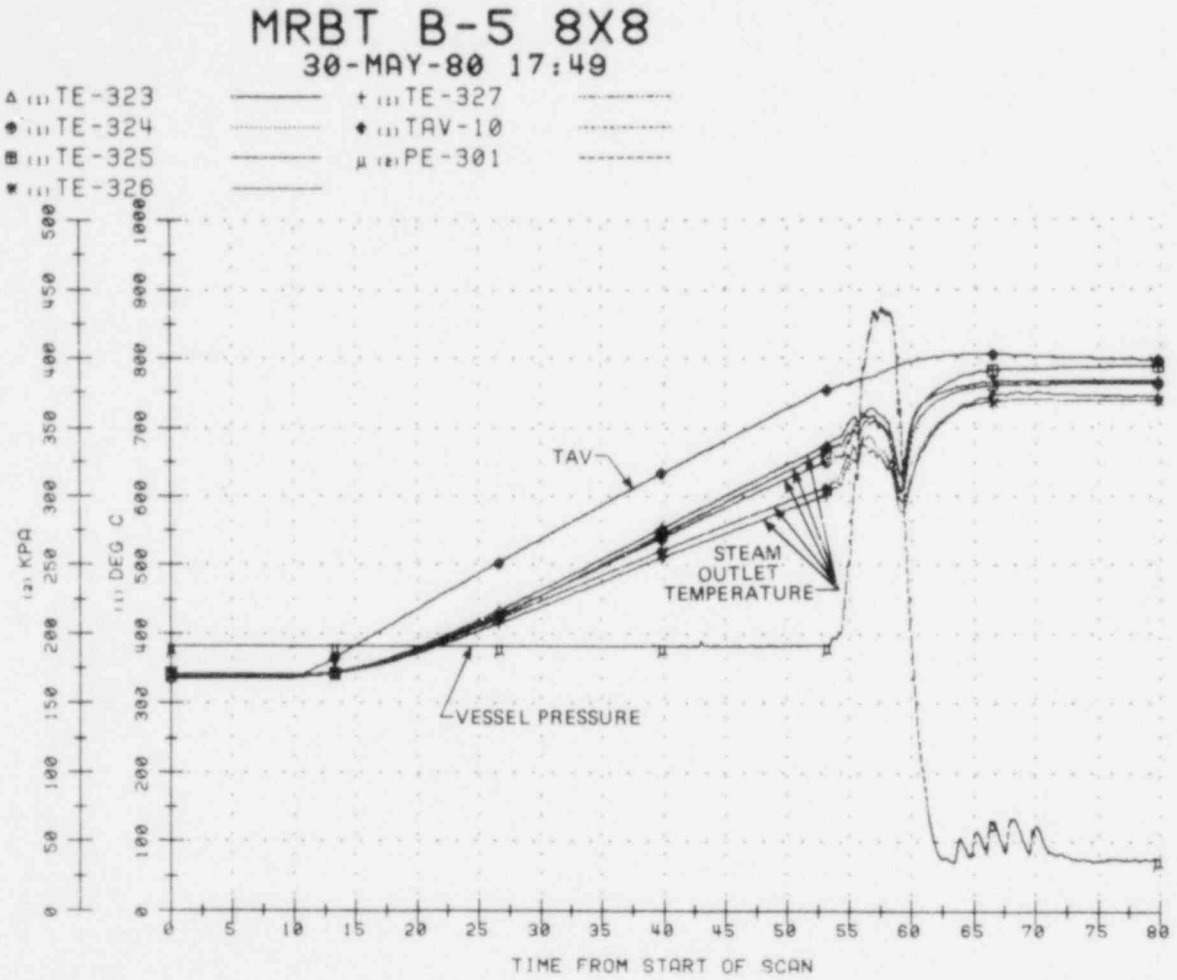

Fig. 21. Steam outlet temperature during test.

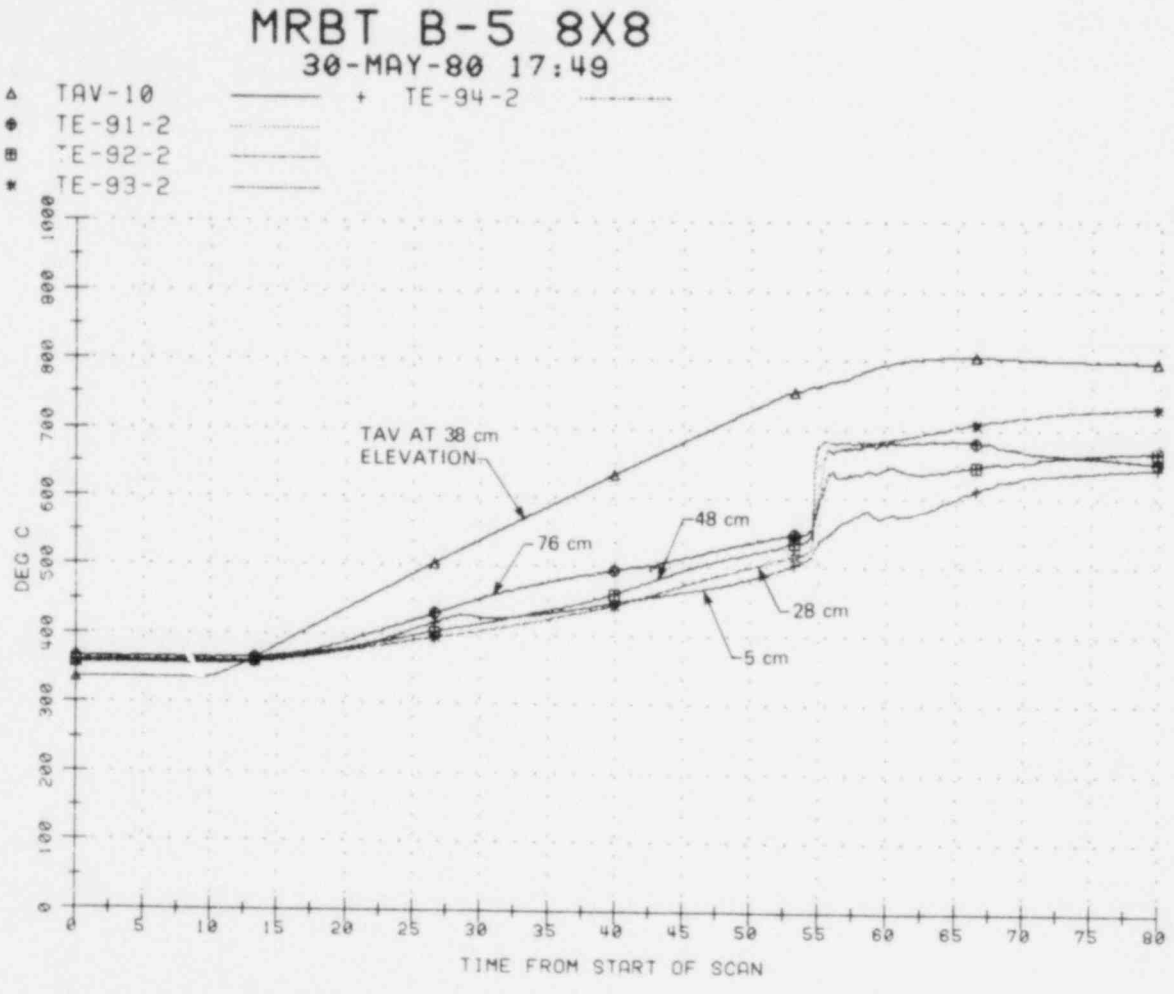

Fig. 22. Shroud temperature measurements on west side of bundle.

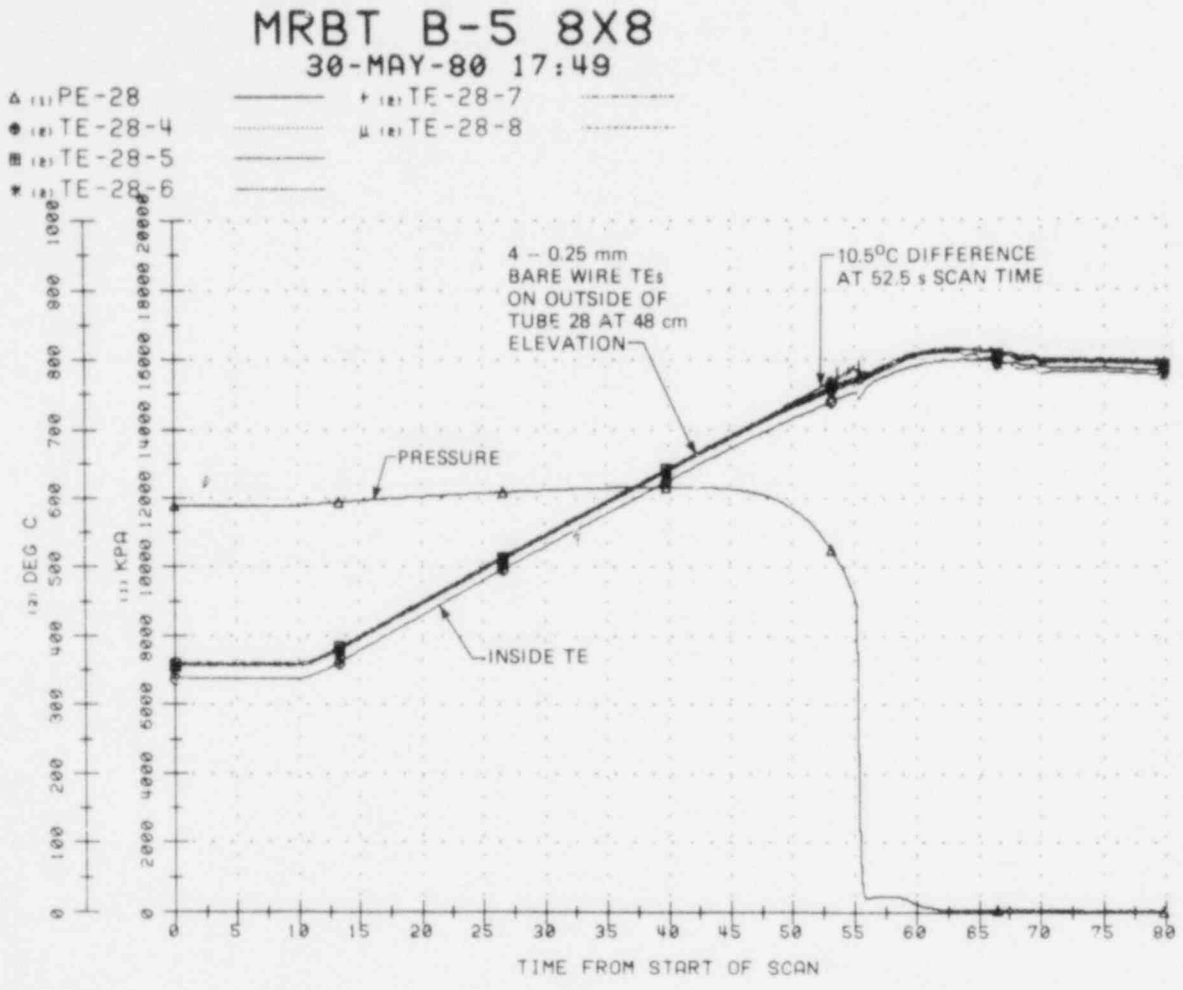

Fig. 23. Azimuthal temperature gradient (Rod 28).

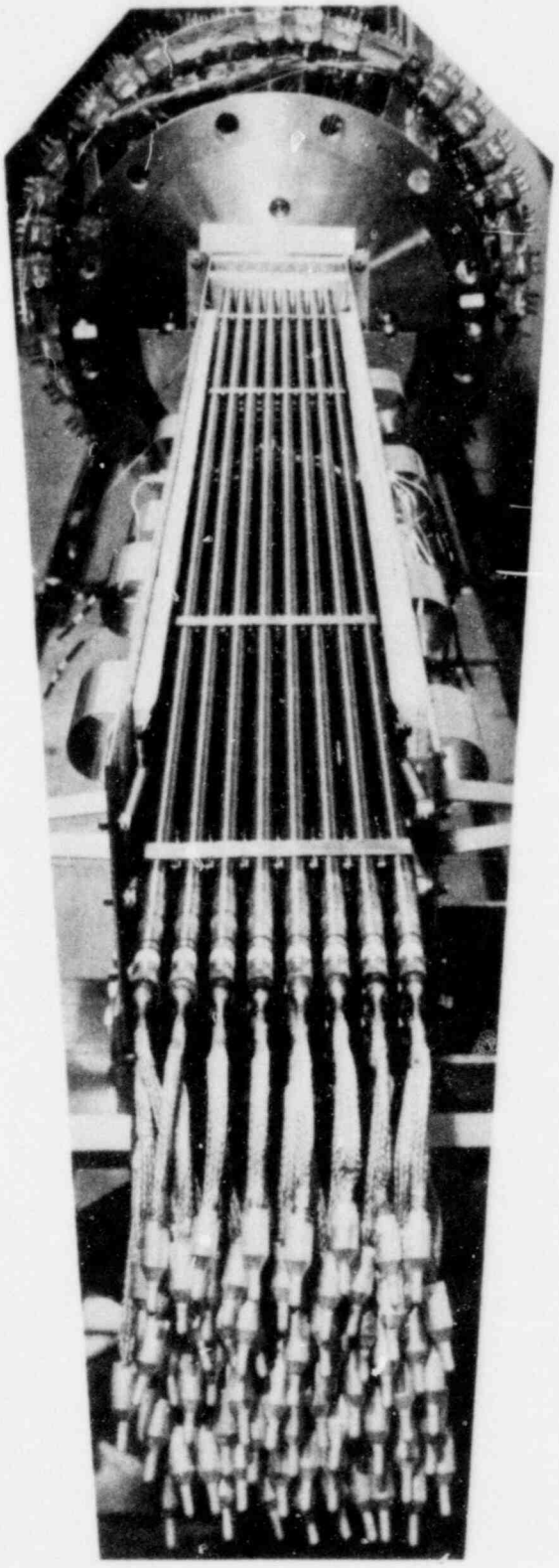

Fig. 24. Pretest view of B-5 before north face of the shroud box was installed.

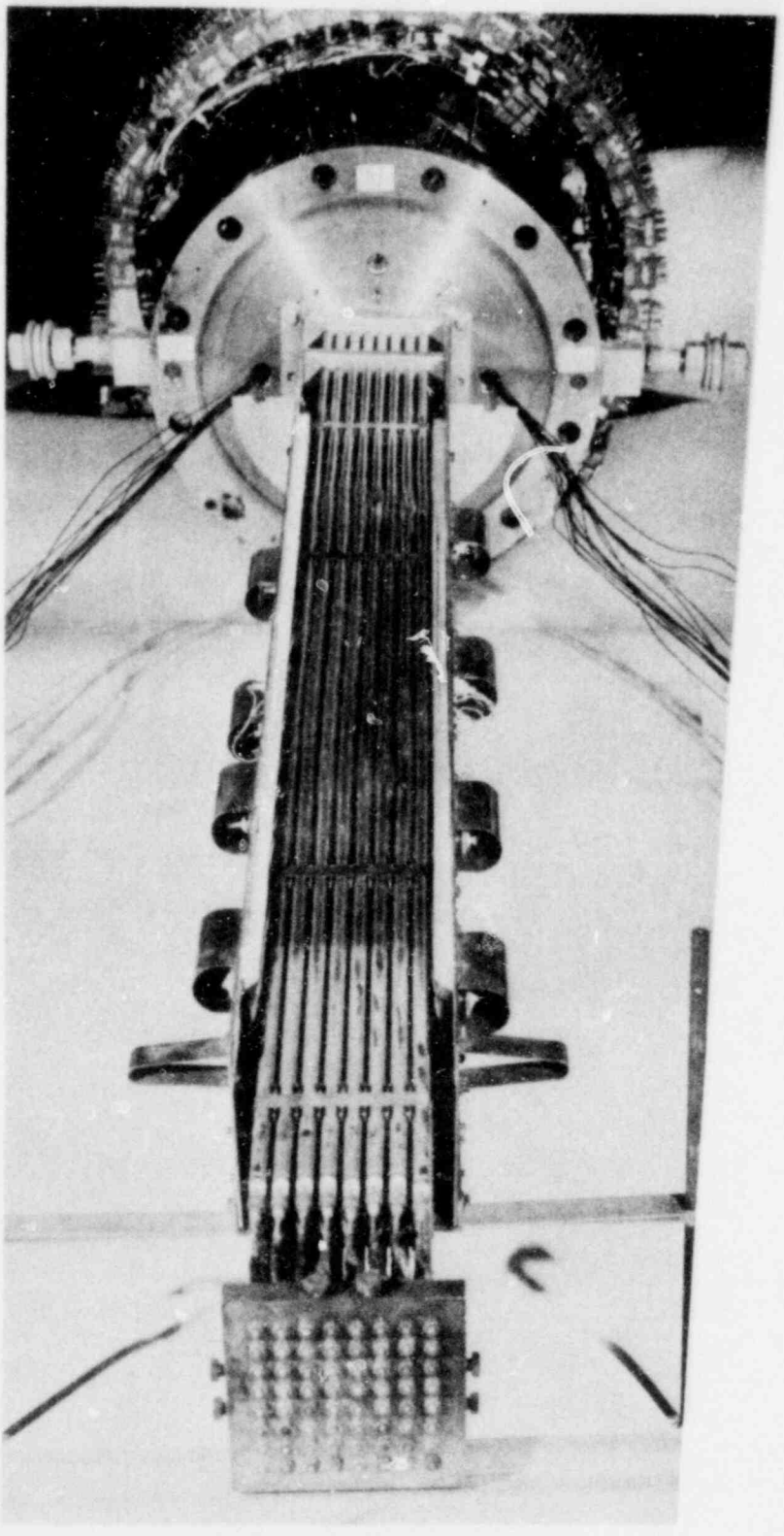

Fig. 25. Posttest view of B-5 after partial disassembly.

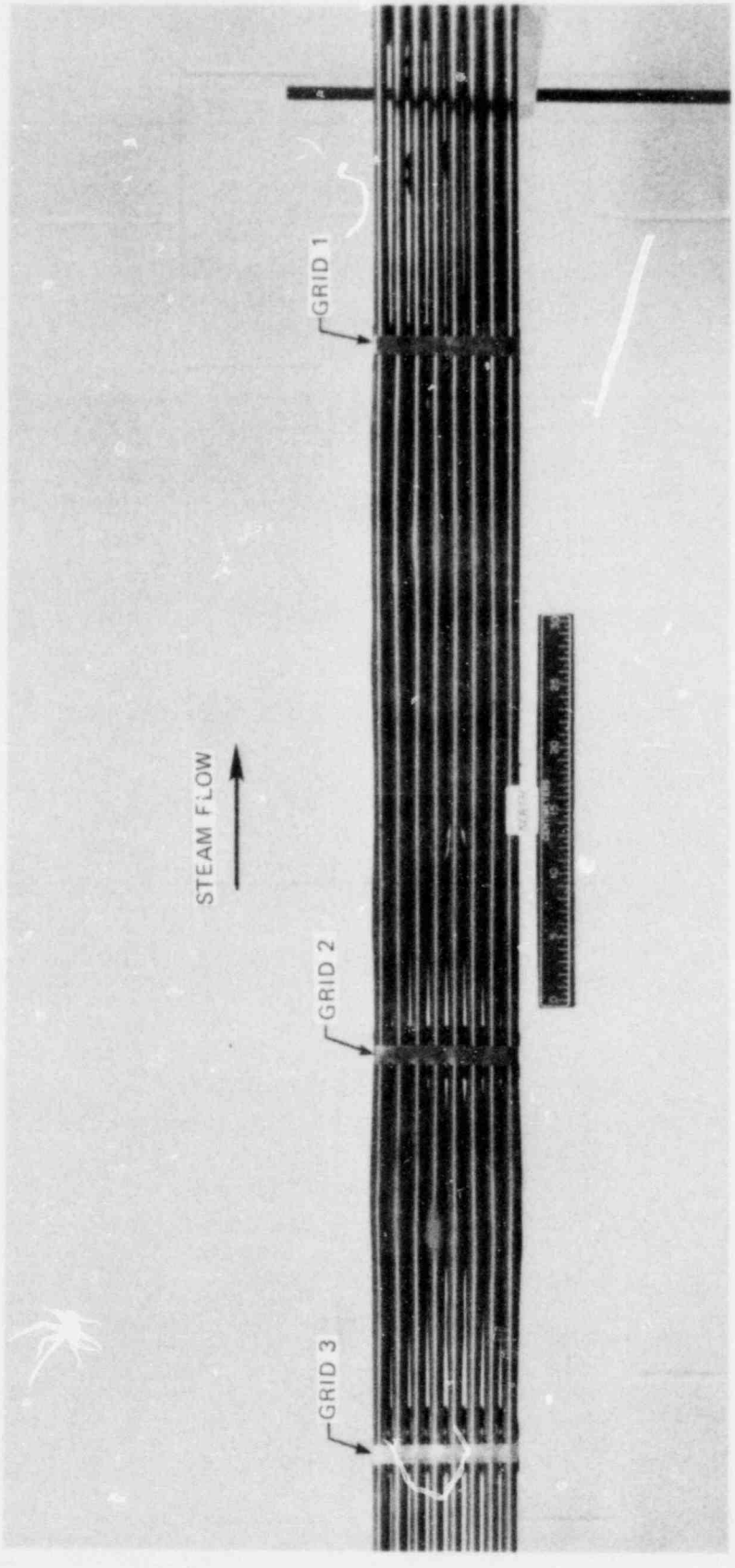

Fig. 26. Posttest view of north face of B-5. West face is up in this view.

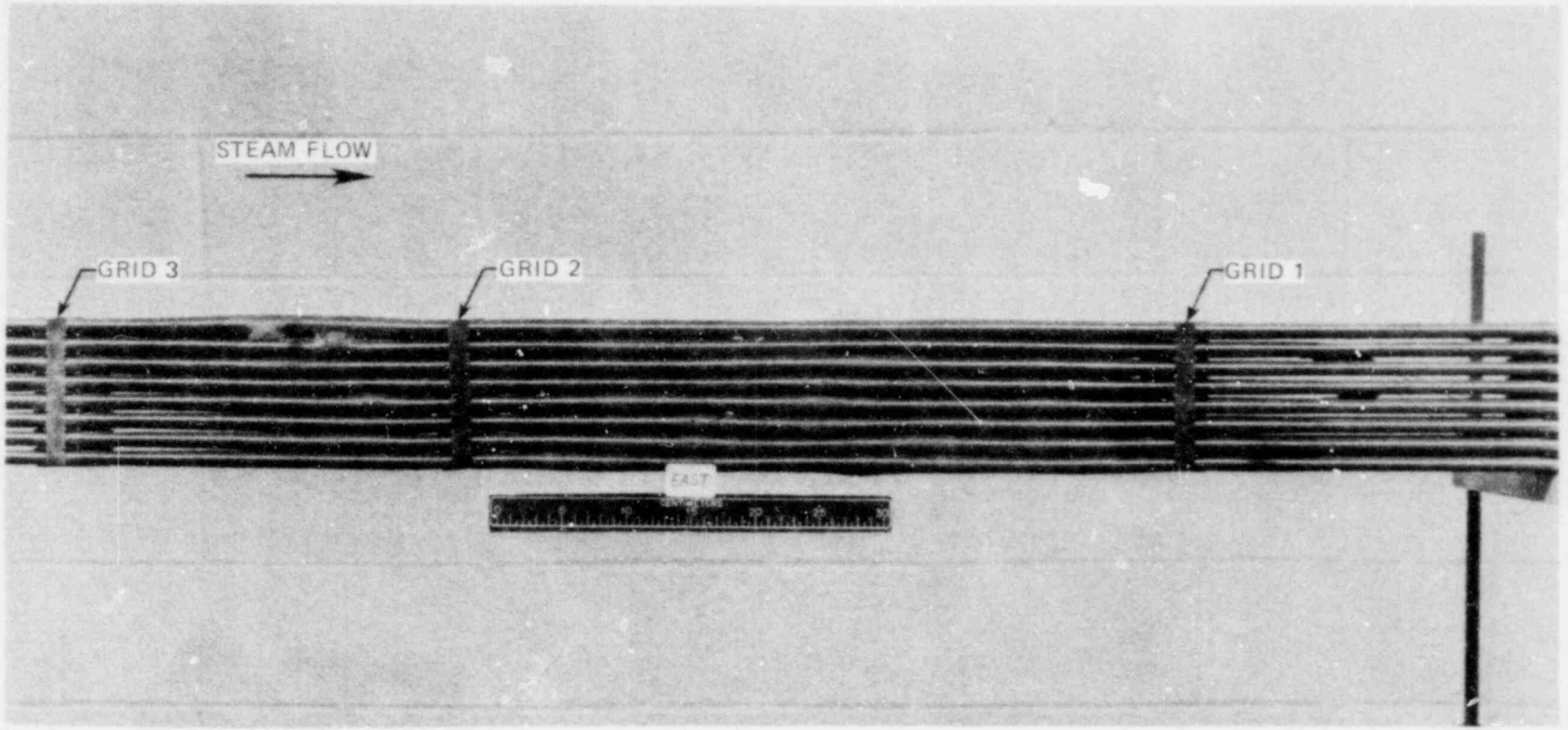

Fig. 27. Posttest view of east face of B-5. North face is up in this view.

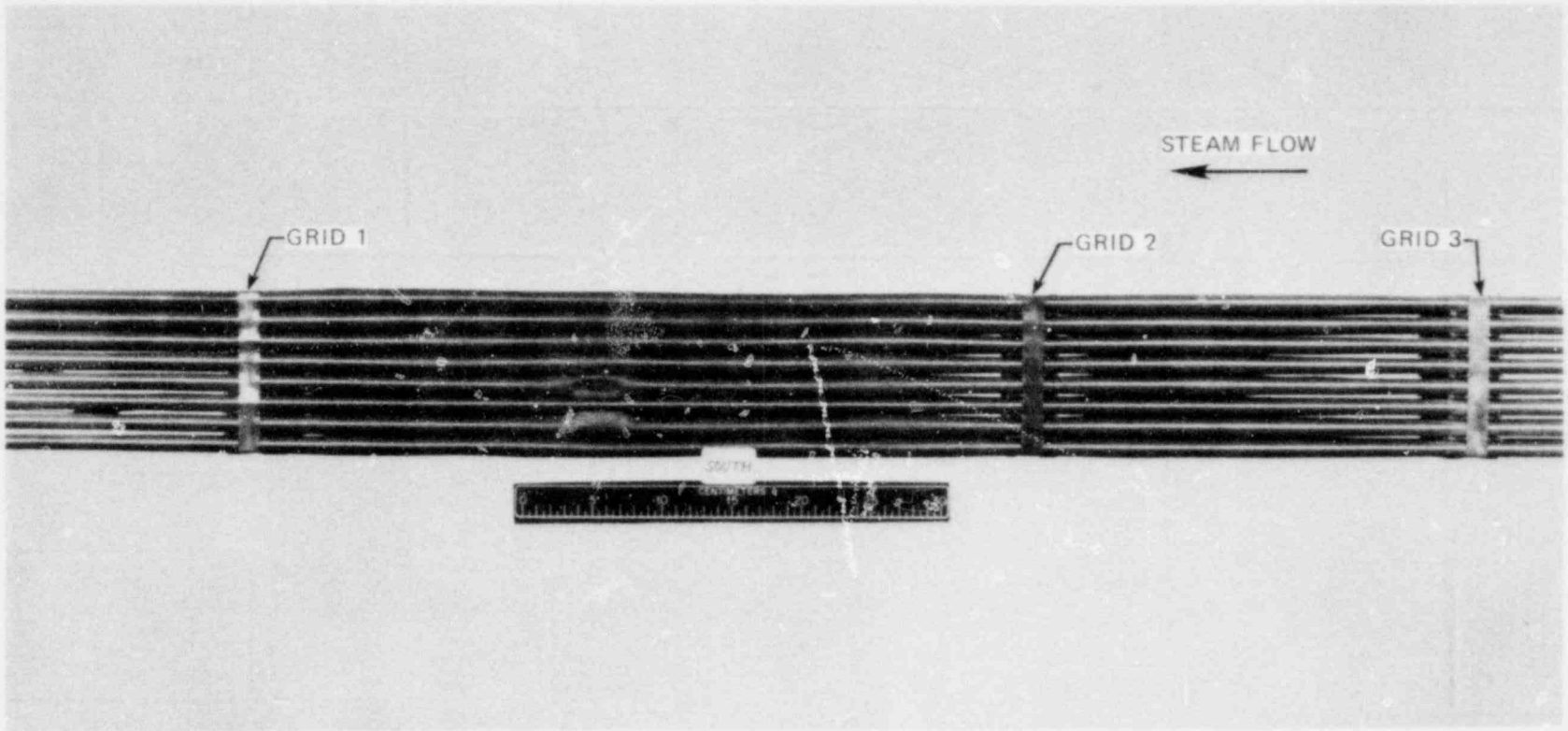

Fig. 28. Posttest view of south face of B-5. West face is up in this view. Note pin position 62 (third up from bottom) which was unpressurized and is underformed.

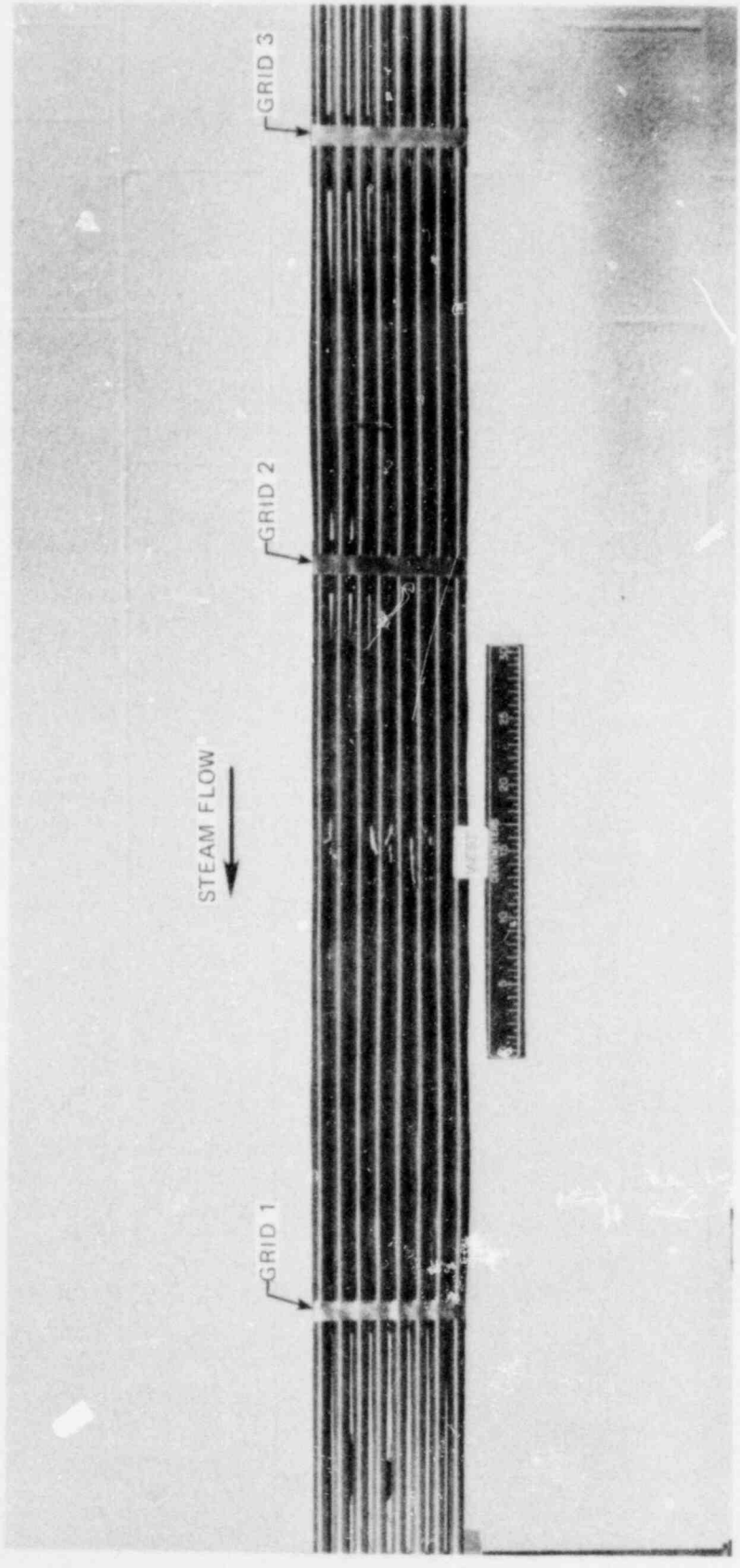

Fig. 29. Posttest view of west face of B-5. North face is up in this view.

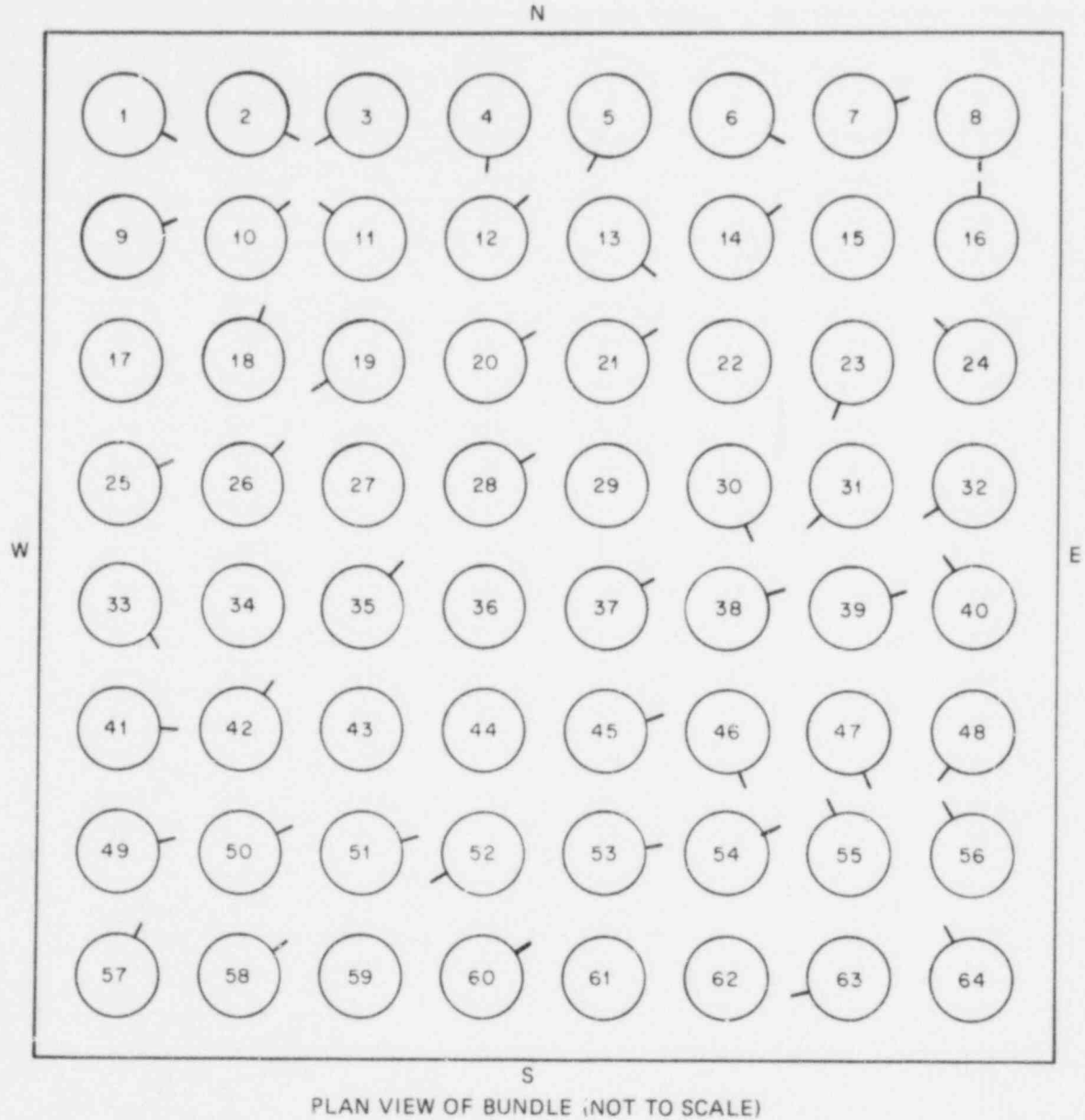

PLAN VIEW OF BUNDLE (NOT TO SCALE)

Fig. 30. Approximate orientation of bursts in B-5 test. Except for tube 62, which was unpressurized and did not burst, tubes without indications retain heaters and determination of burst orientations is impossible at this time.

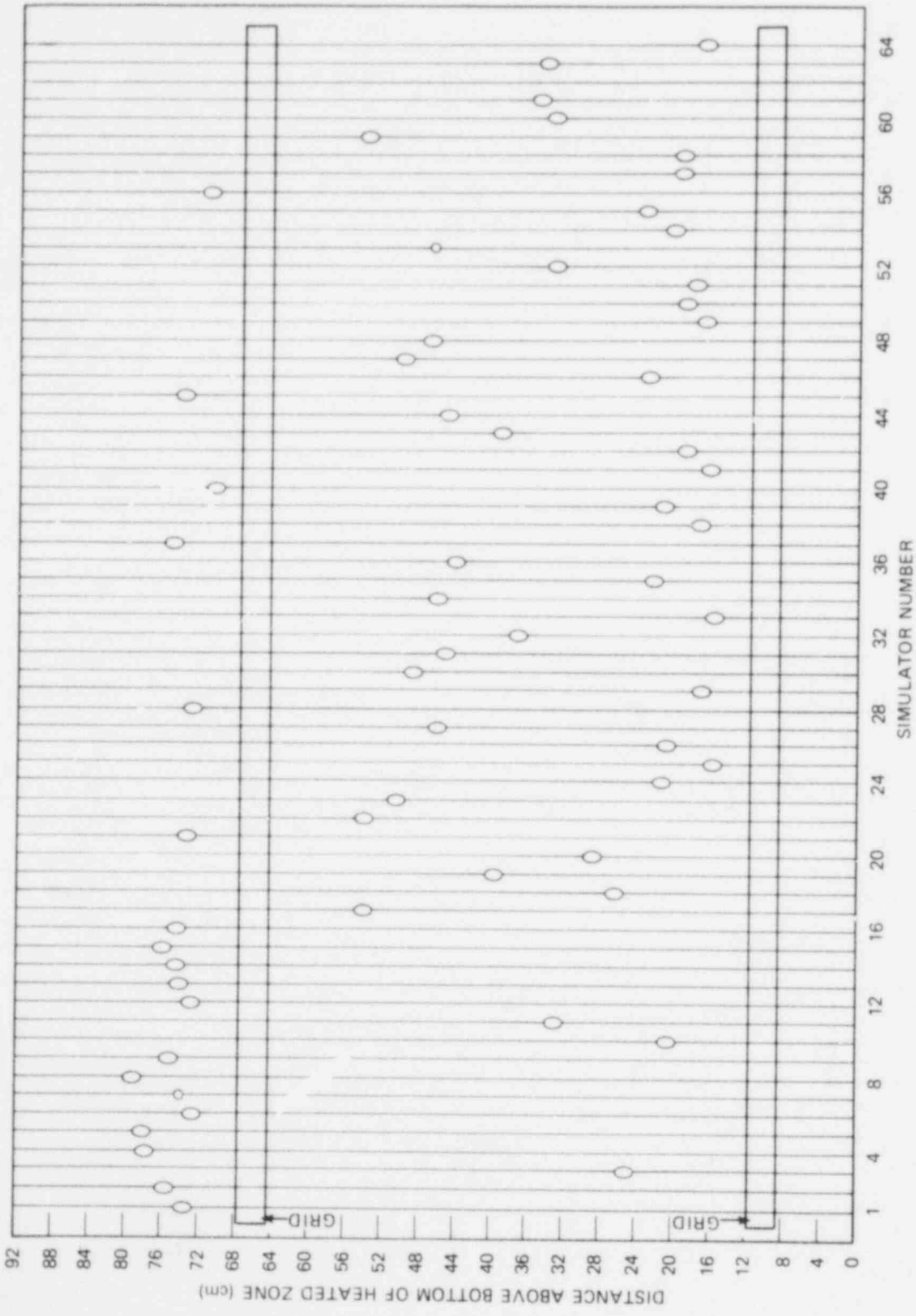

Fig. 31. Approximate axial burst locations in B-5.

Internal Distribution

1. W. A. Bird
2-6. R. H. Chapman
7-8. J. L. Crowley
9. F. R. Gibson
10. R. F. Haynes
11. D. O. Hobson
12. A. W. Longest
13. F. R. Mynatt
14. H. R. Payne
15. R. D. Stulting
16. J. D. White
17. H. E. Trammell
18. D. B. Trauger
19. Laboratory Record Department(RC)

External Distribution

20. Director, Division of Reactor Safety Research, Office of Nuclear Regulatory Research, Nuclear Regulatory Commission, Washington, D.C. 20555
21. Assistant Director, Light Water Reactors, Division of Reactor Safety Research, Office of Nuclear Regulatory Research, Nuclear Regulatory Commission, Washington, D.C. 20555
22. Chief, Fuel Behavior Branch, Division of Reactor Safety Research, Office of Nuclear Regulatory Research, Nuclear Regulatory Commission, Washington, D.C. 20555
23-24. Division of Technical Information and Document Control (NRC-TDIC), Nuclear Regulatory Commission, Washington, D.C. 20555
25-27. Director, Reactor Safety Research Coordination, DOE
28. Assistant Manager, Energy Research and Development, DOE-ORO
29. Director, Nuclear Research and Development Division, DOE-ORO
30-31. Technical Information Center (DOE-TIC), DOE-OR
32-34. Nuclear Regulatory Commission, Washington, D.C. 20555 (Attn: Chief, Core Performance Branch, Division of Systems Safety, Office Nuclear Reactor Regulation, 1 copy; P. A. Boehnert, ACRS, MS H-1016, 1 copy; M. L. Picklesimer, RSR, MS 1130 SS, 1 copy)
35. R. A. Adamson, Mail Code V-03, General Electric Company, Vallecitos Atomic Laboratory, P.O. Box 846, Pleasanton, CA 94566
36. D. L. Burman, Westinghouse Nuclear Fuel Division, P.O. Box 355, Pittsburgh, PA 15230
37. C. E. Crouthamel, Exxon Nuclear, Inc., 2955 George Washington Way, Richland, WA 99352
38. R. R. Hobbins, EG&G Idaho, Inc., INEL, Idaho Falls, ID 83401
39. T. Howe, EG&G Idaho, Inc., INEL, Idaho Falls, ID 83401
40. [illegible]shikawa, Japan Atomic Energy Research Institute, Tokai-Mura, [illegible]a-Gun, Ibaragi-Ken, Japan
41. H. Rininsland, Projekt Nukleare Sicherheit, Kernforschungszentrum, Postfach 3640, 75 Karlsruhe, Federal Republic of Germany

42. T. F. Kassner, Argonne National Laboratory, 9700 South Cass Avenue, Argonne, IL 60439
43. M. Levenson, Electric Power Research Institute, 3412 Hillview Avenue, P.O. Box 10412, Palo Alto, CA 94304
44-45. W. Lowenstein, Electric Power Research Institute, 3412 Hillview Avenue, P.O. Box 10412, Palo Alto, CA 94304
46. A. L. Lowe, Babcock and Wilson Company, P.O. Box 1260, Lynchburg, VA 24505
47. C. L. Mohr, Pacific Northwest Laboratories, P.O. Box 999, Richland, WA 99352
48. J. T. A. Roberts, Electirc Power Research Institute, 3412 Hillview Avenue, P.O. Box 10412, Palo Alto, CA 94304
49. H. Seipel, Der Bundesminister fur Forschung und Technologie, 53 Bonn 12, Postfach 120370, Federal Republic of Germany
50. P. A. Smerd, Combustion Engineering, Inc. 1000 Prospect Hill Road, Windsor, CT 06093
51. H. Zeile, EG&G Idaho Inc., INEL, Idaho Falls, ID 83401